PREPRINT NUMBERS HERE manuscript No.
(will be inserted by the editor)

Precise predictions for same-sign W-bosons scattering at the LHC

Alessandro Ballestrero[8], Benedikt Biedermann[1], Simon Brass[2], Ansgar Denner[1], Stefan Dittmaier[3], Pietro Govoni[4], Michele Grossi[5,6], Alexander Karlberg[7], Ezio Maina[8,9], Mathieu Pellen[1], Giovanni Pelliccioli[8,9], Simon Plätzer[10], Michael Rauch[11], Daniela Rebuzzi[5], Jürgen Reuter[12], Vincent Rothe[12], Christopher Schwan[3], Pascal Stienemeier[12], Marco Zaro[13]

[1]Universität Würzburg, Institut für Theoretische Physik und Astrophysik, Emil-Hilb-Weg 22, 97074 Würzburg, Germany
[2]Universität Siegen, Department Physik, Walter-Flex-Str.3, 57068 Siegen, Germany
[3]Albert-Ludwigs-Universität Freiburg, Physikalisches Institut, Hermann-Herder-Str. 3, 79104 Freiburg, Germany
[4]Milan, Italy
[5]Universitá di Pavia, Dipartimento di Fisica and INFN, Sezione di Pavia, Via A. Bassi 6, 27100 Pavia, Italy
[6]IBM Italia s.p.a. Circonvallazione Idroscalo , 20090 Segrate (MI), Italy
[7]Department of Physics, University of Zürich, 8057 Zürich, Switzerland
[8]INFN, Sezione di Torino, Via P. Giuria 1, 10125 Torino, Italy
[9]Università di Torino, Dipartimento di Fisica, Via P. Giuria 1, 10125 Torino, Italy
[10]Particle Physics, Faculty of Physics, University of Vienna, Vienna, Austria
[11]Institute for Theoretical Physics, Karlsruhe Institute of Technology (KIT), 76131 Karlsruhe, Germany
[12]DESY Theory Group, Notkestr. 85, 22607 Hamburg, Germany
[13]Nikhef, Science Park 105, 1098XG Amsterdam, The Netherlands

the date of receipt and acceptance should be inserted later

Abstract

Vector-boson scattering processes are of great importance for the current run-2 and future runs at design energy of the Large Hadron Collider. The presence of triple and quartic gauge couplings gives access to tests of the gauge sector and possible new-physics contributions there. For this, a precise knowledge of the Standard Model contributions is necessary, which at least matches the experimental uncertainties.

In this article, we present a detailed study of the vector-boson scattering process with two positively charged leptons and missing transverse momentum in the final state, mediated predominantly by same-sign production of two W bosons with positive charge. In particular, we carry out a comparison between the full NLO QCD corrections against several approximations. This study is not only performed in the usual fiducial region used by experimental collaborations, but also in a more inclusive set-up. This allows to infer precisely the quality of such approximations. Finally, we discuss NLO predictions matched to various parton showers. Thanks to this, it is thus possible to infer the systematic errors related to vector-boson scattering at the NLO-QCD level and beyond.

1 Introduction

Vector-boson scattering (VBS) is a class of processes that allow to probe the nature of Higgs-vector-vector couplings and triple and quartic gauge couplings. It is usually understood that VBS refers to the scattering of massive vector-bosons ($W^{\pm}, Z$), which therefore couple to the Higgs boson and can be longitudinally polarised. The scattering of longitudinally polarised bosons is of particular interest, because the corresponding matrix elements feature both gauge and unitarity cancellations that strongly depend on the actual structure of the Higgs sector. A detailed study of this class of processes will therefore further constrain the Higgs couplings and hint at or exclude non-Standard Model Higgs bosons.

The process with two positively charged W bosons is the VBS process with the largest signal-to-background ratio at the LHC, for which evidence has been found in 8 TeV data [1, 2] and which is now started to be observed [3] and measured [4] in 13 TeV data. For now the measurements of VBS processes are limited by statistics but the situation will change in a near future. On the theoretical side, it is thus of prime importance to provide precise predictions and infer their related systematic errors.

The W^+W^+ scattering is the simplest VBS process to calculate, because of the double-charge structure of

the leptonic final state that limits the number of partonic processes and total number of Feynman diagrams for each process. It also implies that irreducible backgrounds are comparatively small, which make this VBS process experimentally favourable in comparison to *e.g.* W^+W^- scattering, which has the largest cross section. Therefore, the W^+W^+ scattering is an ideal candidate for a detailed study of various theoretical predictions.

In the last few years, several next-to-leading order (NLO) computations became available for both the VBS process [5–11] and its QCD-induced irreducible background process [11–15]. The VBS computations all rely on approximations, while recently the complete NLO corrections have been performed [16]. It is therefore interesting to infer in details the quality of the various approximations. Indeed, apart from Ref. [16] where it is commented on, [MP: more references?] no detailed comparison of the VBS approximations have been carried out. Preliminary results of the present study have already been made public in Ref. [17].

The hadronic process is $pp \to \mu^+\nu_\mu e^+\nu_e jj + X$, which includes the W^+W^+ scattering. This final state possesses three contributions at leading order (LO) whose coupling orders are $\mathcal{O}(\alpha^6)$, $\mathcal{O}(\alpha_s\alpha^5)$, and $\mathcal{O}(\alpha_s^2\alpha^4)$. They are commonly referred to as electroweak (EW), interference, and QCD contributions, respectively.[1] Therefore, the present work starts with a LO study of these three contributions as a function of typical VBS cuts. This allows to quantify the various contributions to the final state $\mu^+\nu_\mu e^+\nu_e jj$. This is followed by a LO comparison between the various predictions at the level of the cross section and differential distributions.

At NLO, the process possesses four contributions of orders $\mathcal{O}(\alpha^7)$, $\mathcal{O}(\alpha_s\alpha^6)$, $\mathcal{O}(\alpha_s^2\alpha^5)$, and $\mathcal{O}(\alpha_s^3\alpha^4)$. The largest ones are the EW corrections [16, 18] of order $\mathcal{O}(\alpha^7)$. The contribution to the order $\mathcal{O}(\alpha_s\alpha^6)$ is the second largest NLO contribution and is often referred to as the QCD corrections to the VBS process. In the following, this order is the one where our comparisons are focused on. In this article we will refer to it as simply *NLO*. As for the LO study, the various predictions are compared at the level of the cross section and differential distributions now at NLO accuracy. In particular, this allows to infer the accuracy of the so-called VBS approximation, which we will define in more details later. To our knowledge, such a detailed study was still missing.

Finally, several predictions featuring parton shower are compared. This allows to infer systematic differences between the various predictions. A first study for the W^+W^-jj VBS process has been presented in Ref. [19], comparing the angular-ordered default shower and the dipole shower and bothMC@NLO-like [20] and POWHEG-like [21, 22] matching as implemented in Herwig 7 [23], also showing scale-variation uncertainties. This is the first time in the literature that NLO QCD calculations for VBS processed matched to parton shower are compared between different generators.

Obviously all VBS processes deserve such a detailed study but the present article sets standards for inferring systematics related to NLO corrections and beyond.

The article is organised as follows: First, we define the process under study in Sec. 2. Various approximation at LO and NLO are described in Sec. 3. This is followed by a presentation of the programs used for the computations. Sections 4 and 5 are devoted to a LO and NLO study at fixed order, respectively. Section 6 then adds the effect of parton showers and hadronization to the fixed-order results by matching the two. The last section consists in concluding remarks and recommendations for experimental collaborations.

2 Definition of the process

The scattering of two positively charged W bosons is proceeding at the LHC through the partonic process:

$$pp \to \mu^+\nu_\mu e^+\nu_e jj + X. \tag{1}$$

This process possesses three LO contributions of different orders. The first one is of order $\mathcal{O}(\alpha^6)$ and is referred to as EW contribution. In addition to typical VBS contributions, as shown on the left of Fig. 1, it also features s-channel contributions. Note that we define s-, t-, and u-channel contributions by looking at the process which is contained by only looking at the quark lines, *i.*e. s-channel denotes all Feynman diagrams where the two initial-state partons are connected by a continuous fermion line, and u-channel is the contribution with crossed fermion lines, which appears for identical quarks or anti-quarks in the final state. The s-channels will play a particular role in the study of the various contributions in Sec. 4.1. Some of them take the form of decay chains, for example the diagram represented in the middle of Fig. 1, while others are tri-boson contributions (right of Fig. 1). When using approximations, care must be taken that only gauge-invariant subsets are considered to obtain physically meaningful results. We will discuss the commonly-used possible choices in detail in the next section.

The process can also be mediated via a gluon connecting the two quark lines while the W bosons are radiated off the quark lines. These contributions are of order $\mathcal{O}(\alpha_s^2\alpha^4)$ and feature different kinematical behaviours than the EW contribution. Nonetheless they

[1] The EW contribution is sometimes referred to as the VBS contribution even it possesses non-VBS contributions.

share the same final state and therefore constitute an irreducible background.

Finally, due to the specific colour structure of these two classes of amplitudes, there exist non-zero interferences if only one quark family is involved. These are of order $\mathcal{O}(\alpha_s\alpha^5)$ and are usually small but not negligible for realistic experimental set-ups [16].

In experimental measurements, special VBS-cuts are designed to enhance the EW contribution over the QCD one. These cuts are based on the fact that the two contributions have different kinematical behaviour. The EW contribution is characterised by two jets with large rapidities as well as a large invariant mass. The two W bosons are mostly produced centrally. This is in contrast with the QCD contribution which favours jets in the central region. Therefore, the event selection usually involves rapidity-difference and invariance-mass cuts for the jets. This will be further discussed in Sec. 4.1.

3 Details of the calculations

3.1 Several descriptions for one process

As mentioned previously, the contribution of main interest in our process is the scattering of two W gauge bosons, which includes the quartic gauge-boson vertex. Therefore it is justified to approximate the full EW contributions simply by only these contributions which contain the $2 \to 2$ scattering process as a subpart. However, this set of contributions is not gauge invariant. To make it gauge invariant, one should perform an on-shell projection of the incoming W bosons. Unfortunately, these momenta are space-like and thus a simple on-shell projection is not possible. Instead, one can keep the W boson legs connected to the external quark line off-shell while the ones connected to the final-state leptons, which are already time-like, are put on-shell. Then the polarisation of the gauge boson is accommodated following for example the implementations of Refs. [24, 25]. Such an approximation is usually called effective vector-boson approximation (EVBA) [26–28].

A less crude approximation consists in considering all t- and u- diagrams and squaring them separately, neglecting interference contributions between the two. These interferences are expected to be small in the VBS fiducial region, as they are both phase-space and colour suppressed. The s-channel squared diagrams and any interferences with s-channels are left out as well. This approximation is often called t-/u- approximation, VBF, or even VBS approximation. We will adopt the latter denomination in the following of the article. Such an approximation is implemented at LO in the computer codes Bonsay and Powheg. This approximation is gauge-invariant, which can be seen by considering that the two protons and therefore the two incoming quarks belong to two different, but otherwise identical, copies of the $SU(3)$ gauge group.

The squared matrix element of the s-channel contributions can be added in addition, but all interferences between different kinematic channels are still neglected. This is the level of simulation available in VBFNLO.

All other codes (MG5_aMC, MoCaNLO+Recola, PHANTOM, and Whizard) consider all contributions of order $\mathcal{O}(\alpha^6)$ as well as all possible interferences. Note that the final W boson can always be considered either on-shell or off-shell without affecting the previous discussion. All the codes mentioned here are described in details in the following sub-section.

Moving on to NLO accuracy, one can extend the approximations presented at LO. The VBS approximation at NLO is straightforward for the virtual contributions, for the real-contributions one must be careful about gluon-initiated processes[2]. This is implemented in POWHEG. This approximation can be used in combination with a double-pole approximation [29] for the virtual contribution. Such an approximation is implemented in Bonsay. In VBFNLO, the s-channel contributions are available as well and can be added on top of the VBS approximation. For the real emission diagrams, thereby as simplification the gluon emission is fully modelled only for initial-state radiation. The effect of final-state radiation together with the corresponding virtual contributions is included as a K-factor.

A further refinement is to consider the full real contributions as well as part of the virtual. In particular one can consider only one-loop amplitudes where there is no gluon exchange between the quarks and assuming a cancellation of the infrared (IR) poles. [MP: True? I cannot remember exactly what is included] . [MR: What about gauge invariance? A comment about that would be useful as well.] Such predictions are provided by MG5_aMC.

Finally, when considering the full one-loop amplitude of order $\mathcal{O}(g_s^2 g^6)$ and its corresponding real QCD radiation, other contributions have to be added. Indeed, in order to cancel all infrared (IR) divergences arising, also one-loop amplitudes of order $\mathcal{O}(g^8)$ of EW type and their corresponding QED radiations have to be included. The full computation of order $\mathcal{O}(\alpha_s\alpha^6)$ consists

[2]The initial gluon must not couple to the other initial quark, otherwise there are infrared divergences proportional to s-channels which do not match with the ones found in the virtual contributions. The subset of diagrams where all couplings of the initial state gluon to initial state quark are neglected forms a gauge-invariant subset, with the same argument as presented above. This approach is also fully consistent with the picture of two separate SU(3) copies.

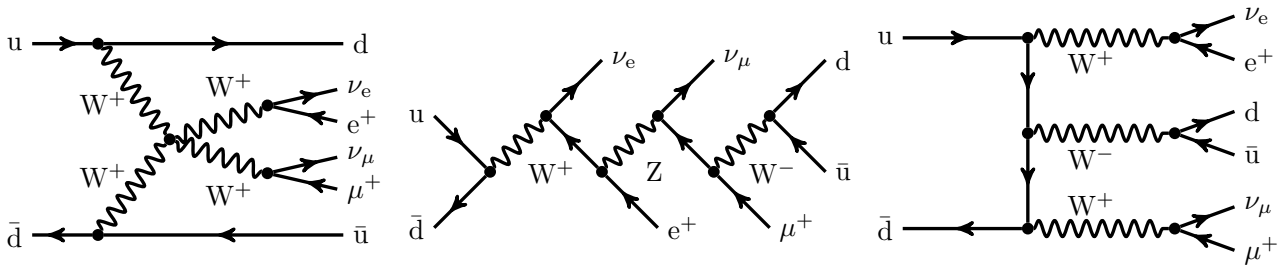

Fig. 1: Sample tree-level diagrams that contribute to the process pp $\to \mu^+\nu_\mu e^+\nu_e jj$ at order $\mathcal{O}(\alpha^6)$. In addition to typical VBS contribution (left), this order also possesses s-channel (middle) and tri-boson contributions (right).

thus not only of QCD-type corrections but also of EW ones.[3] Such predictions are provided by the combination MoCaNLO+Recola as published in Ref. [16].

In Tab. 1 the details of the various codes are reported. In particular, it is specified whether

- all s- and t/u-channel diagrams that lead to the considered final state are included;
- interferences between diagrams are included at LO;
- diagrams which do not feature two resonant vector bosons are included;
- the so-called non-factorisable (NF) QCD corrections, that is the corrections where (real or virtual) gluons are exchanged between different quark lines, are included;
- EW corrections to the $\mathcal{O}(\alpha^5\alpha_s)$ interference are included. These corrections are of the same order as the NLO QCD corrections to the $\mathcal{O}(\alpha^6)$ term.

3.2 Description of the predictions

In the comparison, the following codes are used:

- The program Bonsay consists of a general-purpose Monte Carlo integrator and matrix elements taken from several sources. Born matrix elements are adapted from the program Lusifer [30] for the partonic processes, real matrix elements are written by Marina Billoni, and virtual matrix elements by Stefan Dittmaier. One loop integrals are evaluated using the Collier library [31, 32].
- MadGraph5_aMC@NLO [33] is an automatic meta-code (a code that generates codes) which makes it possible to simulate any scattering process including NLO QCD corrections both at fixed order and including matching to parton showers. It makes use of the FKS subtraction method [34, 35] (automated in the module MadFKS [36, 37]) for regulating IR singularities. The computations of one-loop amplitudes are carried out by switching dynamically between two integral-reduction techniques, OPP [38] or Laurent-series expansion [39], and TIR [40–42]. These have been automated in the module MadLoop [43], which in turn exploits CutTools [44], Ninja [45, 46], or IREGI [47], [MP: Is Collier not missing here? I think it made it to one of the default if I am correct] together with an in-house implementation of the OpenLoops optimisation [48].
  The simulation of VBS at NLO-QCD accuracy can be performed by issuing the following commands in the program interface:

```
> set complex_mass_scheme #1
> import model loop_qcd_qed_sm_Gmu #2
> generate p p > e+ ve mu+ vm j j QCD=0 [QCD] #3
> output #4
```

  With these commands the complex-mass scheme is turned on `#1`, then the NLO-capable model is loaded `#2`[4], finally the process code is generated `#3` (note the `QCD=0` syntax to select the purely-electroweak process) and written to disk `#4`. Because of some internal limitations, which will be lifted in the future version capable of computing both QCD and EW corrections, only loops with QCD-interacting particles are generated. [MP: Detail of the approximation done, divergent part, assumed to cancel etc.]
- Phantom [49] is a dedicated tree-level Monte Carlo for six parton final states at pp, $p\bar{p}$ and e^+e^- colliders at orders α^6 and $\alpha_s^2\alpha^4$ including interferences between the two sets of diagrams. It employs complete tree-level matrix elements in the complex-mass scheme [50] computed via the modular helicity formalism [51, 52]. The integration uses a multichannel approach [53] and an adaptive strategy [54]. Phan-

[3] For more details, the reader is referred to Ref. [16].

[4] Despite the `loop_qcd_qed_sm_Gmu` model also includes NLO counterterms for computing electro-weak corrections, it is not yet possible to compute such corrections with the current version of the code.

Code	$\mathcal{O}(\alpha^6)$ $\lvert s\rvert^2/\ \lvert t\rvert^2/\lvert u\rvert^2$	$\mathcal{O}(\alpha^6)$ interf.	Non-res.	NLO	NF QCD	EW corr. to $\mathcal{O}(\alpha_s\alpha^5)$
Bonsay	t/u	No	Yes, virt. No	Yes	No	No
POWHEG	t/u	No	Yes	Yes	No	No
MG5_aMC	Yes	Yes	Yes	Yes	No virt.	No
MoCaNLO+Recola	Yes	Yes	Yes	Yes	Yes	Yes
PHANTOM	Yes	Yes	Yes	No	-	-
VBFNLO	Yes	No	Yes	Yes	No	No
Whizard	Yes	Yes	Yes	No	-	-

Table 1: Summary of the different properties of the codes employed in the comparison.

tom generates unweighted events at parton level for both the SM and a few instances of BSM theories.

– The Powheg-Box [55, 22] is a framework for matching NLO-QCD calculations with parton showers. It relies on the user providing the matrix elements and Born phase space, but will automatically construct FKS [34] subtraction terms and the phase space for the real emission. For the VBS processes all matrix elements are being provided by a previous version of VBFNLO [56, 57, 15] and hence the approximations used in the Powheg-Box are the similar to those used in VBFNLO. [MP: Mention the non-clustering for the scale as well as the different running of alphas at NLO.]

– The program MoCaNLO+Recola is made of a flexible Monte Carlo program dubbed MoCaNLO and of the matrix element generator Recola [58, 59]. It can compute arbitrary processes for the LHC at both NLO QCD and EW accuracy in the Standard Model. This is made possible by the fact that Recola can compute arbitrary processes at tree and one-loop level in the Standard Model. To that end, it relies on the Collier library [31, 32] to numerically evaluate the one-loop scalar and tensor integrals. In addition, the subtraction of the IR divergences appearing in the real corrections has been automatised thanks to the Catani–Seymour dipole formalism for both QCD and QED [60, 61]. The code has demonstrated its ability to compute at NLO high multiplicity processes up to $2 \to 7$ [62, 63]. In particular the full NLO corrections to VBS and its irreducible background [18, 16] have been obtained from this tool. One key aspect for these high multiplicity processes is the fast integration which is ensured by using similar phase-space mappings to those of Refs. [64, 65, 30].

– VBFNLO [56, 57, 15] is a flexible parton-level Monte Carlo for processes with electroweak bosons. It allows the calculation of VBS processes at NLO QCD in the VBS approximation, with process IDs between 200 and 290. The corresponding s-channel contributions are available separately as triboson processes with semi-leptonic decays, with process IDs in the 400 range. These can simply be added on top of the VBS contribution, as interferences between the two are neglected. The usage of leptonic tensors in the calculation, pioneered in Ref. [5], thereby leads to a significant speed improvement over automatically generated code. Besides the SM, also a variety of new-physics models including anomalous couplings of the Higgs and gauge bosons can be simulated.

– Whizard [66, 67] is a multi-purpose event generator with the LO matrix element generator O'Mega. It provides FKS subtraction terms for any NLO process, while virtual matrix elements are provided externally by OpenLoops [48] (alternatively, Recola [58, 59] (cf. above) can be used as well). Whizard allows to simulate a huge number of BSM models as well, in particular for new physics in the VBS channel in terms of both higher-dimensional operators as well as explicit resonances.

3.3 Input parameters

The VBS production mechanism is simulated at the LHC with a center-of-mass energy $\sqrt{s} = 13\,\text{TeV}$. The NNPDF 3.0 parton density [68] with five flavour scheme, NLO QCD evolution, and a strong coupling constant $\alpha_s(M_Z) = 0.118$ is employed.[5] Since the employed PDF set has no photonic density, photon-induced processes are not considered. Initial-state collinear singularities are factorised with the $\overline{\text{MS}}$ scheme, consistently with what is done in NNPDF.

[5] The corresponding `lhaid` in LHAPDF6 [69] is 260000.

For the mass and width of the massive particles, the following values are used:

$$\begin{aligned} m_{\mathrm{t}} &= 173.21\,\mathrm{GeV}, & \Gamma_{\mathrm{t}} &= 0\,\mathrm{GeV}, \\ M_{\mathrm{Z}}^{\mathrm{OS}} &= 91.1876\,\mathrm{GeV}, & \Gamma_{\mathrm{Z}}^{\mathrm{OS}} &= 2.4952\,\mathrm{GeV}, \\ M_{\mathrm{W}}^{\mathrm{OS}} &= 80.385\,\mathrm{GeV}, & \Gamma_{\mathrm{W}}^{\mathrm{OS}} &= 2.085\,\mathrm{GeV}, \\ M_{\mathrm{H}} &= 125.0\,\mathrm{GeV}, & \Gamma_{\mathrm{H}} &= 4.07 \times 10^{-3}\,\mathrm{GeV}. \end{aligned} \tag{2}$$

The measured on-shell (OS) values for the masses and widths of the W and Z bosons are converted into pole values for the gauge bosons ($V = \mathrm{W}, \mathrm{Z}$) according to Ref. [70],

$$\begin{aligned} M_V &= M_V^{\mathrm{OS}} / \sqrt{1 + (\Gamma_V^{\mathrm{OS}}/M_V^{\mathrm{OS}})^2}\,, \\ \Gamma_V &= \Gamma_V^{\mathrm{OS}} / \sqrt{1 + (\Gamma_V^{\mathrm{OS}}/M_V^{\mathrm{OS}})^2}. \end{aligned} \tag{3}$$

The EW coupling is renormalised in the G_μ scheme [71] where

$$G_\mu = 1.16637 \times 10^{-5}\,\mathrm{GeV}^{-2}. \tag{4}$$

The numerical value of α, corresponding to the choice of input parameters is

$$\alpha = 7.555310522369 \times 10^{-3}. \tag{5}$$

The CKM-Matrix is assumed to be diagonal, meaning that the mixing between different quark families is neglected. The complex-mass scheme [65, 72] is used throughout to treat unstable intermediate particles in a gauge-invariant manner.

The renormalisation and factorisation scales are set to the dynamical scale

$$\mu_{\mathrm{ren}} = \mu_{\mathrm{fac}} = \sqrt{p_{\mathrm{T,j_1}}\, p_{\mathrm{T,j_2}}}. \tag{6}$$

This choice of scale has been shown to provide stable NLO-QCD predictions [10].

Following experimental measurements [1, 4, 2, 73], the event selection used in the present study is:

- The two same-sign charged leptons are required to have

$$p_{\mathrm{T},\ell} > 20\,\mathrm{GeV}, \qquad |y_\ell| < 2.5, \qquad \Delta R_{\ell\ell} > 0.3\,. \tag{7}$$

- The total missing transverse energy, computed from the vectorial sum of the transverse momenta of the two neutrinos, is required to be

$$E_{\mathrm{T,miss}} = p_{\mathrm{T,miss}} > 40\,\mathrm{GeV}\,. \tag{8}$$

- QCD partons (quarks and gluons) are clustered together using the anti-k_T algorithm [74] with distance parameter $R = 0.4$. Jets are required to have

$$p_{\mathrm{T,j}} > 30\,\mathrm{GeV}, \qquad |y_{\mathrm{j}}| < 4.5, \qquad \Delta R_{\mathrm{j}\ell} > 0.3\,. \tag{9}$$

  Typically, on the two jets with largest transverse-momentum VBS cuts are applied. These are an invariant-mass cut on the di-jet system as well as rapidity-separation cut between the two jets. The nominal value of these cuts if not stated explicitly read:

$$m_{\mathrm{jj}} > 500\,\mathrm{GeV}, \qquad |\Delta y_{\mathrm{jj}}| > 2.5. \tag{10}$$

- When EW corrections are computed, real photons and charged fermion are clustered together using the anti-k_T algorithm with radius parameter $R = 0.1$. In this case, leptons and quarks are understood as *dressed fermions*.

4 Leading-order study

4.1 Three contributions

At tree level, there are three contributions to the $\mathrm{W^+W^+}$ production in association with two jets: the pure EW component $\mathcal{O}(\alpha^6)$, the interference $\mathcal{O}(\alpha_{\mathrm{s}}\alpha^5)$, and the QCD background $\mathcal{O}(\alpha_{\mathrm{s}}^2\alpha^4)$. In the present section, the cross sections and distributions are obtained without applying the VBS cuts on m_{jj} and $|\Delta y_{\mathrm{jj}}|$. In Tab. 2, the cross sections of the three contributions are reported. The EW, QCD, and interference contributions amount to 57%, 37%, and 6% of the total inclusive cross section, respectively. The QCD contribution does not posses external gluons due to charge conservation. Thus the $\mathcal{O}(\alpha_{\mathrm{s}}^2\alpha^4)$ diagrams only involve gluon exchange in the t/u-channel between the quark lines. This results in a small contribution although the VBS cuts have not been imposed. The interference between EW and QCD contributions is small, due to color suppression, but not negligible (t/u interference with identical fermions).

Order	$\mathcal{O}(\alpha^6)$	$\mathcal{O}(\alpha_{\mathrm{s}}^2\alpha^4)$	$\mathcal{O}(\alpha_{\mathrm{s}}\alpha^5)$
σ[fb]	2.292 ± 0.002	1.477 ± 0.001	0.223 ± 0.003

Table 2: Cross sections at LO accuracy for the three contributions to the process $\mathrm{pp} \to \mu^+\nu_\mu \mathrm{e}^+\nu_{\mathrm{e}}\mathrm{jj}$. These results are for the set-up described in Sec. 3.3, dropping the m_{jj} and $|\Delta y_{\mathrm{jj}}|$ cuts.

In Fig. 2 these three contributions are shown separately and summed in the differential distribution of the di-jet invariant mass m_{jj} and the rapidity difference

$|\Delta y_{\rm jj}|$. In the distributions in the di-jet invariant mass (left), one can observe that the EW contribution peaks around an invariant mass of about 80 GeV. These are due to diagrams where the two jets originate from the decay of a W boson (see middle and right diagrams in Fig. 1). Note that these contributions are not present in calculations relying on the VBS approximation. Also, the EW contribution becomes dominant for di-jet invariant mass larger than 500 GeV. The same holds true for jet rapidity difference larger than 2.5 (right). This clearly explains why these two observables are used to enhanced the EW contribution over the QCD one. In particular, in order to have a large EW contribution, rather exclusive cuts are required.

This can also be seen in Fig. 3 where the three contributions are displayed as a function of the di-jet invariant mass and jet rapidity difference. Again, it is obvious that the region with low di-jet invariant mass and low jet-rapidity difference should be avoided. This motivates in particular the choice of $m_{\rm jj} > 200\,{\rm GeV}$ and $|\Delta y_{\rm jj}| > 2$ for our inclusive study (see below). Finally, let us notice that the choice $m_{\rm jj} > 500\,{\rm GeV}$ and $|\Delta y_{\rm jj}| > 2.5$ made by the experimental collaborations is well motivated in order to enhance the EW contribution over its irreducible backgrounds. These are the cuts used in Sec. 4.3.

4.2 Inclusive comparison

As explained previously, the low di-jet invariant mass and low jet rapidity separation is dominated by tri-boson production. Therefore, a comparison of the various approximations in an *inclusive* phase-space volume should exclude the region where tri-boson contributions are dominating. To that end, we have chosen for the inclusive fiducial volume to take the following values for the VBS cuts:

$$m_{jj} > 200\,{\rm GeV} \qquad \text{and} \qquad |\Delta y_{jj}| > 2. \tag{11}$$

In Fig. 4, the ratio of double-differential cross sections in the plan $(m_{\rm jj}, \Delta y_{\rm jj})$. Two plots are displayed: the ratio of the $|t|^2 + |u|^2$ and $|s|^2 + |t|^2 + |u|^2$ approximations over the full calculation, respectively. In the first case, the approximation is good within $\pm 10\%$ over the whole range apart in the low invariant-mass region at both low and large rapidity difference. The low rapidity difference region possesses remnants of the tribosons contributions. It is therefore expected that the $|t|^2 + |u|^2$ approximation fails in this region. The second plot, where the $|s|^2 + |t|^2 + |u|^2$ approximation is considered, displays a better behaviour in the previously mentioned region. The full calculation is approximated at the level of $\pm 10\%$ everywhere apart in the upper left corner where the inclusion of s-channel contributions did not improve the approximation. This is due to ... [MP: Ideas?]

4.3 Comparison in the fiducial region

In Tab. 3, we report the total rates at LO accuracy obtained with the set-up described in Eqs. (7-9) with the VBS cuts $m_{\rm jj} > 500\,{\rm GeV}$ and $|\Delta y_{\rm jj}| > 2.5$ (see Eq. (10)). The order considered here is the order $\mathcal{O}(\alpha^6)$. We note that several full predictions are not in statistical agreement. These are possibly due to too aggressive estimations of statistical uncertainty or ... [MP: To be added] Nonetheless, all these predictions agree within less than 0.5%. At the level of the cross section, it seems difficult to infer the quality of the the various approximations. This simply means that the various VBS approximations are not worth than 0.5% at the level of the fiducial cross section at LO for a typical phase-space volume used by experimental collaborations.

Code	σ[fb]
Bonsay	$X \pm 0.0002$
MG5_aMC	$X \pm 0.001$
MoCaNLO+Recola	1.4347 ± 0.0001
PHANTOM	1.4374 ± 0.0006
POWHEG	1.44092 ± 0.00009
VBFNLO	1.43796 ± 0.00005
Whizard	1.4381 ± 0.0002

Table 3: Cross sections for the LHC process $pp \to \mu^+\nu_\mu e^+\nu_e jj$ at LO accuracy and order $\mathcal{O}(\alpha^6)$. The uncertainties shown refers to the estimated statistical error of the Monte Carlo programs. The predictions are obtained in the fiducial region described in Sec. 3.3. [MP: Please add or check your respective numbers]

In Fig. 5, we show the distributions in the invariant mass (top) and the rapidity difference of the two tagging jets (bottom) which are key observables for VBS measurements. In both cases we show the absolute distributions in the upper plot, while the lower plot displays the ratio over VBFNLO [MP: To be changed to Recola] . For both observables we find a relatively good agreement among the various tools, which confirms the fact that contributions from s-channel diagrams as well as from non-resonant configurations are suppressed in the fiducial region. In general, the agreement is at the level of 1% or below for each bin. We have checked that the same level of agreement holds for other standard differential distributions such as rapidity, invariant mass, or transverse momentum. This means that at LO, in

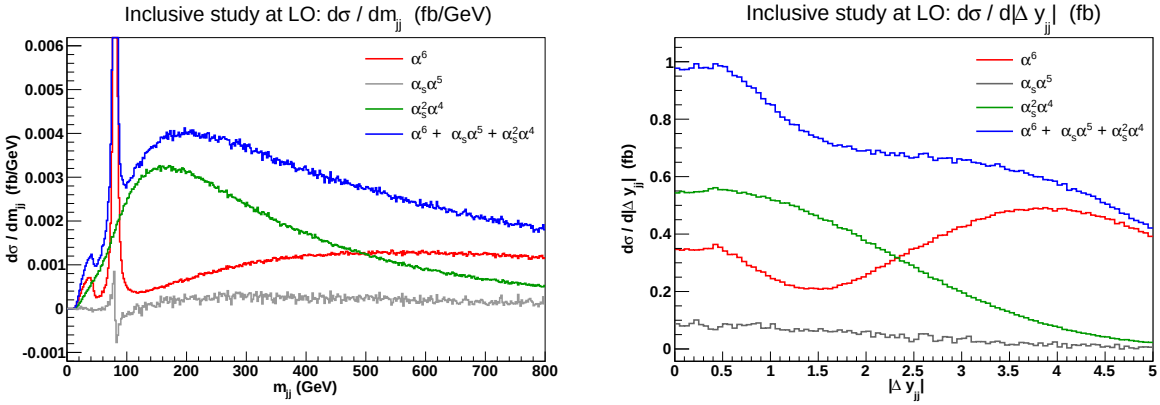

Fig. 2: Differential distribution in the di-jet invariant mass $m_{\rm jj}$ (left) and the difference of the jet rapidities $|\Delta y_{\rm jj}|$ (right) at LO. The EW contribution is in red, the QCD one in green, and the interference in grey. The sum of all the contributions is in blue. No cuts on $m_{\rm jj}$ and $|\Delta y_{\rm jj}|$ are applied. [MP: On the plots: it should be α and not α_{em} and $m_{\rm jj}$ instead of M_{jj}. And we have the convention to put $\alpha_{\rm s}$ before α.]

the fiducial volume, the VBS approximation is good to a per cent. [MP: Add some comment with respect to the 2D scan.]

5 Next-to-leading order QCD

5.1 Inclusive comparision

We now present an inclusive study performed at NLO QCD for the EW component, namely the order $\mathcal{O}(\alpha_{\rm s}\alpha^6)$.

According to the results shown in Sec. 4.2, the VBS approximation at LO fails in the region $m_{\rm jj} < 200$ GeV, $|\Delta y_{\rm jj}| < 2$. For the inclusive region (see Eq. (11)), this approximation is good up to $\pm 10\%$ apart for large di-jet differences and low di-jet invariant mass. It is therefore interesting to check how good this approximation performs at NLO. Thus, we impose the same kinematic cuts shown in Sec. 3.3 and apply the VBS cuts of Eq. (11).

We compare three different predictions at NLO QCD: the VBS approximation ($|t|^2 + |u|^2$) implemented in Bonsay, the VBS approximation with the s-channel contributions ($|s|^2 + |t|^2 + |u|^2$) from VBFNLO, and the full computation. The full computation employs full matrix elements meaning that $t/u/s$ interferences, factorisable, and non-factorisable QCD corrections as well as EW corrections to the order $\mathcal{O}(\alpha_{\rm s}\alpha^6)$ are included. The total cross sections within the above mentioned kinematic cuts are shown in Tab. 4.

The VBS approximation for NLO QCD predictions (labelled by $|t|^2 + |u|^2$) is lower by about 10% with respect to the full calculation. The inclusion of s-channel diagrams improves the approximate prediction down to a 2%-level.

Prediction	$\sigma_{\rm tot}$ [fb]	δ
full	1.8120 ± 0.0144	-
$\lvert t\rvert^2 + \lvert u\rvert^2$	1.6292 ± 0.0001	-10%
$\lvert s\rvert^2 + \lvert t\rvert^2 + \lvert u\rvert^2$	1.7780 ± 0.0001	-2%

Table 4: Total cross sections at NLO QCD *i.e.* at order $\mathcal{O}(\alpha_{\rm s}\alpha^6)$ for the full computation and two approximations. In addition to the cuts of Sec. 3.3, the VBS cuts take the values: $m_{\rm jj} > 200\,\text{GeV}$ and $|\Delta y_{\rm jj}| > 2$.

These differences are much more evident in differential distributions. In Fig. 6, we show the distributions in the di-jet invariant mass $m_{\rm jj}$ and rapidity separation $|\Delta y_{\rm jj}|$. For large $m_{\rm jj}$ and large $|\Delta y_{\rm jj}|$, as expected, the VBS approximation is performing well and its s-channel extension agree with the full calculation within 10% per cent. This is in contrast with the region $200\,\text{GeV} < m_{\rm jj} < 500\,\text{GeV}$ and $2 < |\Delta y_{\rm jj}| < 2.5$, the discrepancy between the $|t|^2 + |u|^2$ approximation and the full computation goes up to 30%. The inclusion of s-channels cures partly the discrepancy in this region. Still, for the very low $m_{\rm jj}$ a difference of about 5% remains. This might indicate that also interferences (GP: and non–factorizable QCD corrections ? [MP: I don't know, we have to think about it]) are needed in this phase-space region.

In order to investigate further the jet-pair kinematics, we look at the double-differential distribution in the variables $m_{\rm jj}$ and $\Delta y_{\rm jj}$. In particular, we compute in each bin the ratio of the approximated cross sections over the full one. In Fig. 7 and Fig. 8 we show the ratio $\sigma(|t|^2 + |u|^2)/\sigma(\text{full})$ and $\sigma(|s|^2 + |t|^2 + |u|^2)/\sigma(\text{full})$, respectively.

As expected, in the low invariant mass–low rapidity separation region of the jet pair the VBS approximation fails significantly (up to 40% discrepancies). The inclusion of the s-channel brings the difference down to at most 5%. However, the positive discrepancy shown in the low m_{jj} region (black curve on the upper plots of Fig. 6) can be traced back to the low m_{jj}, large Δy_{jj} region of Fig. 8. In this region, the two leading jets have soft transverse momenta, according to the following low-angle approximation

$$\begin{aligned} m^2_{\mathrm{j}_i\mathrm{j}_j} &= 2\, p_{\mathrm{T},\mathrm{j}_i} p_{\mathrm{T},\mathrm{j}_j} \left(\cosh \Delta y_{\mathrm{j}_i\mathrm{j}_j} - \cos \Delta\phi_{\mathrm{j}_i\mathrm{j}_j}\right) \\ &\approx 2\, p_{\mathrm{T},\mathrm{j}_i} p_{\mathrm{T},\mathrm{j}_j} \cosh \Delta y_{\mathrm{j}_i\mathrm{j}_j} \ . \end{aligned} \tag{12}$$

The same positive discrepancy for the $|s|^2 + |t|^2 + |u|^2$ approximation, can be seen in the low p_{T} region of the leading jet in the upper plot of Fig. 9. In the large invariant mass–small rapidity separation region of Fig. 8, discrepancies at the level of 15% are present. This can be traced back to the large p_{T} and central rapidity region of the leading jets kinematics, shown in Fig. 9. For such distributions, despite the s-channel inclusion, the discrepancy between the approximated and full result is of about $5-10\%$. In the VBS signal-region the VBS approximation shows a good agreement with the full calculation as documented in details below.

Concerning leptonic observables, we show in Fig. 10 the distributions of the lepton-lepton invariant mass and of the Zeppenfeld variable of the electron. It is defined as

$$z_{\mathrm{e}^+} = \frac{y_{\mathrm{e}^+} - \frac{y_{\mathrm{j}_1}+y_{\mathrm{j}2}}{2}}{|y_{\mathrm{j}_1} - y_{\mathrm{j}_2}|} \ . \tag{13}$$

Analogous definitions will later also be used for the Zeppenfeld variable of the muon and of the third jet. The VBFNLO result for the $e^+\mu^+$ invariant mass agrees rather well with the full curve, obtained from MoCaNLO+Recola. The prediction from Bonsay is about 10% lower. The discrepancies are roughly constant over the whole spectrum. Instead, the right panel of Fig. 10 clearly shows that the Zeppenfeld variable of the positron z_e is strongly affected by the exclusion of s-channels, with increasing discrepancy with respect to the full result at large values. The muon observable z_μ behaves identically to the electron one, z_e.

In conclusion, both the loose minimum di-jet invariant mass cut and the inclusion of QCD radiative correction make the s-channel contributions less suppressed than at LO, making their inclusion mandatory, in order to provide trustworthy predictions at NLO accuracy. Nevertheless, interferences and non-factorizable QCD corrections should be included to reduce the discrepancies down to about 1%, mainly in inclusive analyses. Instead, the VBS approximation at NLO provides a good approximation of full calculations in the kinematic region where VBS contributions are dominant ($M_{\mathrm{jj}} \gtrsim 600\,\mathrm{GeV}$, $|\Delta y_{\mathrm{jj}}| \gtrsim 3$), for both total cross section and differential distributions.

5.2 Comparison in the fiducial region

In Tab. 5, the cross sections of the various tools at NLO-QCD accuracy are presented. The order considered is again the order $\mathcal{O}(\alpha_{\mathrm{s}}\alpha^6)$ and the fiducial volume is the one described in Sec. 3.3. In contrast with Tab. 3, the NLO predictions are visibly differ according to the approximations used.

Code	σ[fb]
Bonsay	$X \pm 0.0009$
MG5_aMC	$X \pm 0.003$
MoCaNLO+Recola	1.382 ± 0.002
POWHEG	1.3556 ± 0.0009
VBFNLO	1.3916 ± 0.0001

Table 5: Cross sections for the LHC process $\mathrm{pp} \to \mu^+\nu_\mu \mathrm{e}^+\nu_{\mathrm{e}}\mathrm{jj}$ at NLO accuracy and order $\mathcal{O}(\alpha^6)$. The uncertainties shown refers to estimated statistical error of the Monte Carlo programs. The predictions are obtained in the fiducial region described in Sec. 3.3.
[MP: Please add or check your respective numbers.]
[MR: My t-/u-channel-only number is 1.3703(1), so something additionally must be going on with Powheg, which we should comment on.]

The first observation is that the predictions featuring two versions of the VBS approximation (Bonsay and POWHEG) are close. This means that the double-pole approximation on the two W bosons used in Bonsay constitutes a good approximation of the VBS-approximated virtual corrections implemented in POWHEG. Both predictions differ by about 2% with respect to the full computation (MoCaNLO+Recola). The second observation is that the inclusion of s-channel contributions seems to have a significant impact. Indeed, its inclusion (as done in VBFNLO) approximates the full computation by less than a per-cent (0.7%). The main source of the s-channel diagrams thereby consists of real-emission contributions, where one of the two leading jets is formed by one quark, or possibly also both quarks, originating from the W decay, and the second one by the extra radiation emitted from the initial state. In such configurations, the hadronically decaying W boson can become on-shell and hence yield larger

contributions than at LO, where the invariant mass cut on the two jets forces the boson into the far off-shell region.

In Figs. (11-13), several differential distributions are shown. All these predictions are performed at NLO accuracy at the order $\mathcal{O}(\alpha_s\alpha^6)$. [MP: Physics and conclusion on interference/non-factorisable etc. effects are not addresses yet in the discussion.]

We start with Fig. 11 which displays the invariant mass (top) and the rapidity separation (bottom) of the two tagging jets. For high invariant mass, all predictions agree rather well. On the other hand, for low invariant mass, the hierarchy present at the level of the cross section is here reproduced. The VBS-approximated predictions (BONSAY and POWHEG) are lower than the full calculation (MoCaNLO+Recola). The full calculation is rather well approximated by the hybrid VBS approximation implemented in MadGraph5_aMC@NLO. Finally, VBFNLO which include as well s-channel contributions provides larger predictions at low invariant mass. For the rapidity difference between the two tagging jets, the hierarchy between the predictions is rather similar.

Concerning the transverse momentum (top) and rapidity (bottom) of the hardest jet shown in Fig. 12, the situation is rather different. While MadGraph5_aMC@NLO is very close to the full prediction for low transverse momentum, it is diverging from it at larger transverse momentum. This is in contrast with BONSAY and POWHEG which approximate the full computation reasonably well over the whole range and in particular in the high transverse-momentum region. Finally, VBFNLO predicts higher rates over the whole range apart around 200 GeV where it is in perfect agreement with the complete calculation. Concerning the rapidity of the hardest jet, VBFNLO is in good agreement with MoCaNLO+Recola in the rapidity range $|y_{j_1}| < 3$. For larger rapidity, the other codes constitute a better description of the full process at order $\mathcal{O}(\alpha_s\alpha^6)$.

The last set of differential distributions is the invariant mass of the two charged lepton (top) and the Zeppenfeld variable for the anti-muon (bottom). Concerning the comparison of the predictions, both distributions display a rather similar behaviour. Indeed, the hierarchy mentioned previously is here respected and enhanced towards high invariant mass or high Zeppenfeld variable. MoCaNLO+Recola and VBFNLO are in rather good agreement for both distributions for the kinematic range displayed here. The other three VBS approximations are close to each other within few per cent.

6 Matching to parton shower

We now discuss how different predictions compare when the matching to parton-shower (PS) is included. For such a comparison we expect larger discrepancy than what we found at fixed-order, as a consequence of the different matching schemes, parton shower employed and of other details of the matching (such as the choice of the parton shower initial scale). Among the codes capable of providing fixed-order results, presented before, MG5_aMC, POWHEG, and VBFNLO can also provide results at (N)LO+PS accuracy. For VBFNLO, we restrict ourselves to showing results only in the VBS approximation, *i*.e. the s-channel contributions are neglected here. Besides, also PHANTOM is employed for LO+PS results.
MG5_aMC, which employs the MC@NLO [20] matching procedure, will be used together with Pythia8 [75] (version 2.2.3) and Herwig++ [76, 77] (version 2.7.1). For POWHEG, the homonymous [MP: Is it the correct word? Because it would mean that the work "Powheg" has different meaning. Isn't it?] matching procedure is employed [21, 22], together with Pythia8 **MZ VERSION? if same as MG5, put it at the end together with the tune**. VBFNLO serves as a matrix-element and phase-space provider for the Matchbox module [78] of Herwig7 [23, 79], using an extended version of the BLHA interface [80–82]. The Matchbox module makes it possible to choose between MC@NLO-like and POWHEG-like matching. As parton shower, both the default angular-ordered shower as well as the dipole shower can be employed. Finally, PHANTOM results will be shown matched with Pythia 8 and Herwig++. Whenever Pythia8 is used, the Monash tune [83] is selected.

Results will be presented within the cuts described in Sec. 3.3, applied after shower and hadronisation (this implies that jets are obtained by clustering stable hadrons, and not QCD partons). It follows that at the event-generation level, looser cuts (or even no cuts at all) must be employed in order not to bias the results. **MZ lepton-jet separation at the hard-event level?**.

Compared to the fixed order computations, a slightly different set-up has been employed for MG5_aMC in order to simplify the calculation: instead of generating the full $pp \to \mu^+\nu_\mu e^+\nu_e jj$ process, since it is anyway dominated by doubly-resonant contribution, the events are produced for the process with two stable W^+ bosons ($pp \to W^+W^+jj$), and these W^+ bosons are decayed with MadSpin [84] (keeping spin correlations) before the PS. Since MadSpin computes the partial and total decay width of the W bosons at LO accuracy only, while in Section 3.3 the NLO width is employed, a small

effect (6%) on the normalisation of distribution is induced. Finally, when the renormalisation and factorisation scales are set, the $\Delta R_{j\ell}$ cut is not imposed during the jet-clustering procedure, but this has no visible effect on the results [MP: Is it true? Because I remember some numbers from Christopher with 1% or so] .

Code	σ[fb]
MG5_aMC+Pythia8	1.450(1.368) ± 0.004
MG5_aMC+Herwig++	1.445(1.363) ± 0.004
POWHEG	1.3642 ± 0.0004
VBFNLO+Herwig7-Dipole	1.3389 ± 0.0006
VBFNLO+Herwig7-Default	1.3067 ± 0.0006
MG5_aMC+Pythia8 (LO)	1.352(1.275) ± 0.003
MG5_aMC+Herwig++ (LO)	1.343(1.267) ± 0.003
PHANTOM+Pythia8	1.235 ± 0.001
PHANTOM+Herwig++	1.260 ± 0.001
VBFNLO+Herwig7 (LO)	1.3001 ± 0.0002

Table 6: Rates at NLO-QCD (LO-QCD) accuracy matched to parton shower within VBS cuts obtained with the different codes used in this comparison, for the $pp \to \mu^+\nu_\mu e^+\nu_e jj$ process. Numbers in parentheses for the MG5_aMC simulations are rescaled to account for the effect related to the boson widths computed by MadSpin (see the text for details).

We now present the results of predictions matched to parton shower: the total rates within VBS cuts are displayed in Table 6, both at LO and NLO accuracy. For MG5_aMC, the numbers in parentheses are rescaled to take into account the width effects described in the above paragraph. Once this effect is taken into account, total rates from different tools agree within few per cent. Larger discrepancies however will appear for differential observables, which we are going to discuss in the following. For any observable, results will be presented in two plots, shown side-by-side. In the plot on the left (right), (N)LO+PS predictions are shown with different colours in the main frame. In the inset, these predictions are compared in both cases with a fixed-order prediction at NLO accuracy (obtained with VBFNLO *i.e.* the VBS approximation with s-channel contributions). For the differential observables, the MG5_aMC predictions are *not* rescaled to compensate for the width effect mentioned above.

The first observable we investigate is the exclusive jet multiplicity, shown in Fig. 14. Looking at the LO+PS predictions, one can appreciate that the main effects are driven by the parton shower that is employed Herwig++/7 or Pythia8, with the clear tendency of producing more radiation for the latter, leading to higher jet multiplicities. Difference among tools that employ the same parton shower are typically smaller, and can be traced back to different values of the initial scale of the parton shower. The main effect of NLO corrections for this (rather inclusive) observable is to stabilise the predictions for the two-jet bin, where discrepancies among tools are reduced to about 10%. For the three-jet bin, which is described only at LO accuracy, differences among tools remain large: the largest rate is predicted by MG5_aMC, while the smallest rate is predicted by Powheg, both matched to Pythia8. Despite the fact that the same parton shower is employed, the way emissions are treated is different among the two tools. In particular, for Powheg, the first emission is generated with an internal Sudakov form factor (the prediction dubbed Powheg-no shower corresponds to stopping after the first emission), while for MG5_aMC there is an interplay between the real-emission matrix element and the shower emission.

The next observable that we study is the invariant mass of the two tagging jets, shown in Fig. 15. For this observable, both at LO+PS and NLO+PS, the spread of predictions matched with parton shower is rather small ($\lesssim 10\%$, if one compensates for the 6% width effect for MG5_aMC); LO+PS predictions tend to be significantly softer than the fixed NLO one, with an effect of about -30% at the end of the displayed range. At NLO+PS, this effect is much more mitigated, owing to the better description of the first QCD emission which is now driven by the real-emission matrix element.

The rapidity difference between the two tagging jets, shown in Fig. 16 has some similarities to the invariant-mass distribution: at LO+PS all predictions, except for VBFNLO3+Herwig7 where the effect is mitigated, show the tendency to deplete the large-separation region with respect to the fixed-order prediction, in a quantitatively similar way. At NLO+PS, when the extra radiation is described by the real matrix element, such an effect is greatly reduced. A notable exception is the Powheg prediction, which still shows a suppression at large separations: since such a suppression is already there for the Powheg-no shower sample, it is very likely that it is driven by the way the first emission is generated. A minor effect in the same direction is visible in the last two bins of the MG5_aMC+Herwig++ prediction (although with rather large statistical uncertainties).

The transverse momentum of the hardest and second-hardest jets are shown in Figures 17 and 18 respectively. In general, for both observables, predictions from different tools agree rather well with each other, with a spread at most at the 10% level. At LO+PS, typically the transverse-momentum spectra are softer than the fixed-NLO ones, and this effect is more marked for the second-hardest jet which, as expected, is more sensitive

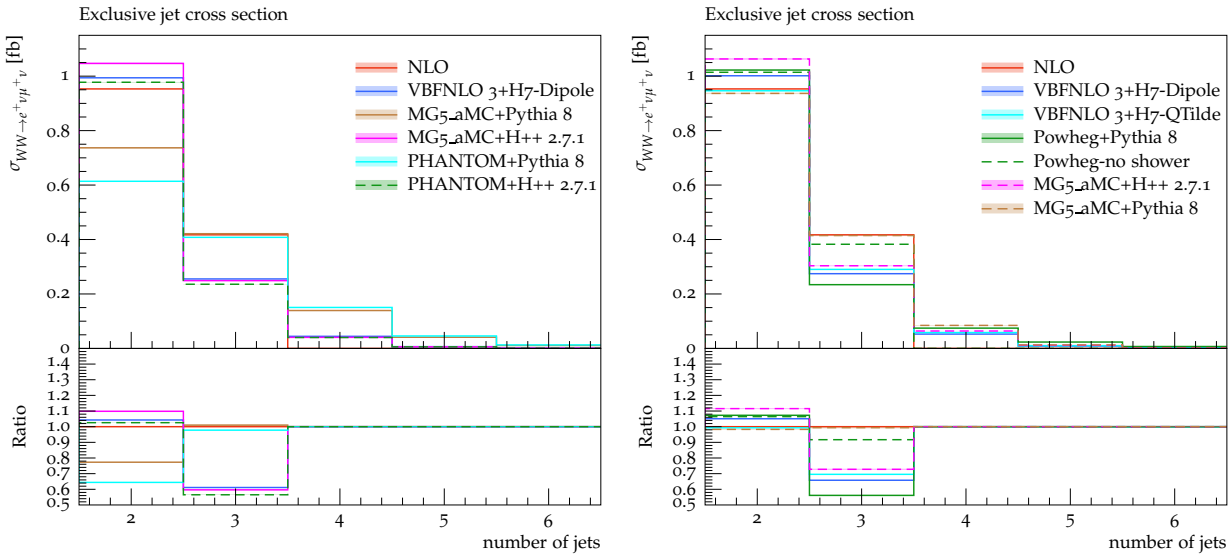

Fig. 14: Exclusive jet multiplicity from predictions matched to parton shower, at LO (left) or NLO (right) accuracy, compared with the fixed-NLO result computed with VBFNLO

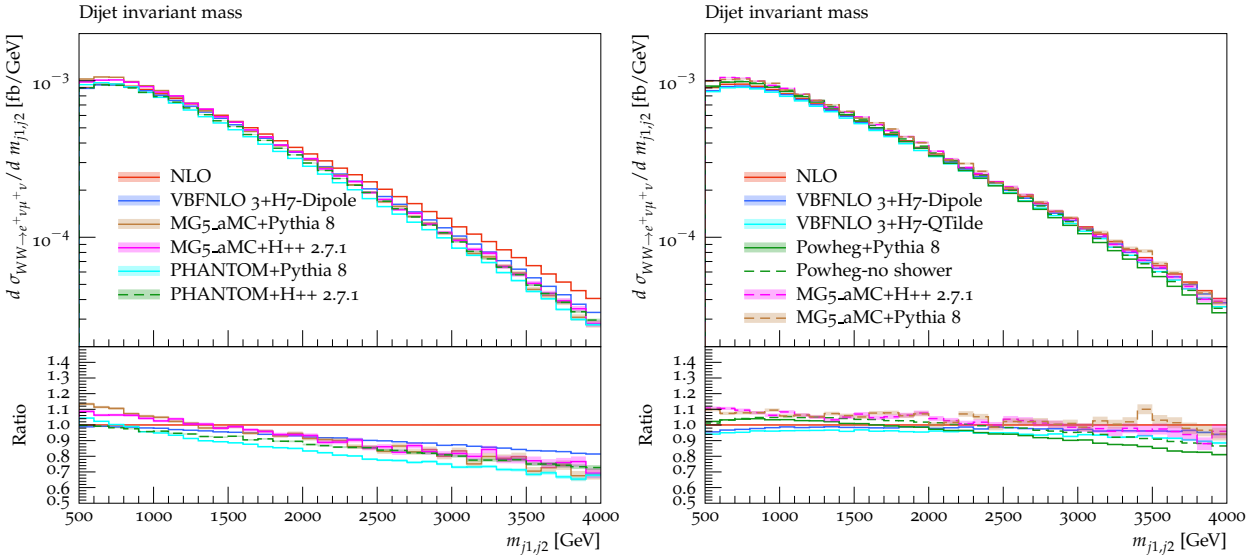

Fig. 15: Same as in Fig. 14, for the invariant mass of the two tagging jets.

to the description of the extra radiation. Again, this effect is mitigated by NLO corrections. The only feature that may be worth noticing among the NLO+PS predictions is the tendency of POWHEG to suppress the hardest-jet spectrum at low transverse momentum ($p_{\mathrm{T,j_1}} < 100\,\mathrm{GeV}$).

If we consider the rapidity of the second jet, Fig. 19, we observe again rather small differences among tools, with the tendency towards a general stabilisation at NLO+PS. However, some (small) differences in the shape remain at NLO+PS, which are worth to be briefly discussed: predictions obtained with MG5_aMC are very close to the fixed-order prediction; POWHEG displays an enhancement of the central region, and a consequent suppression in the peripheral region, while VBFNLO shows an opposite behaviour. However, the effect is rather small, with the largest departure from the fixed-order prediction being at most 10%.

Finally, focusing on the third jet, we conclude the list of differential observables with the rapidity and the Zeppenfeld variable defined in Eq. (13), Figures 20 and 21. **MZ the rapidity can be dropped (check also the following discussion in case)** In general, for observables which involve the third jet, one can

clearly see a degradation of the agreement among the various tools, because of the poorer perturbative description of these observables. The rapidity and Zeppenfeld variable z are a striking example: both at LO and NLO, the tendency of Pythia8 to generate more hard and central radiation (corresponding to low values of z) is clearly visible; it is interesting to notice that this effect survives beyond the first emission, as it can be observed by comparing Powheg-no shower with Powheg+Pythia8. If it is true that the central enhancement is a bit mitigated if NLO+PS tools are used (compare LO+PS and NLO+PS from MG5_aMC+Pythia8 with the fixed-NLO prediction), however even at NLO+PS the central region ($z_{j_3} < 0.5$) is cursed by huge differences between tools. Large differences, reaching a factor 2, persist also away from the central region.

In conclusion, the comparison of tools including matching with parton-shower clearly shows the benefits of the inclusion of NLO corrections: for most observables described effectively at NLO accuracy differences between tools are at (or below) the 10% level. **MZ compare this number with scale uncertainties** Some exceptions exist, *e.g.* the rapidity separation of the two tagging jets, which on the one hand clearly suggest not to rely on a single tool/parton shower, and on the other make it worth to investigate more in details the way QCD radiation is generated **MZ cite here H VBF at NNLO?**. Finally, the size of discrepancies for observables that are described at a lower perturbative accuracy, notably those related to the third jet, suggest that experimental analyses should rely as least as possible on those observables and, in any case, use conservative estimate of the theory uncertainties. In order to improve the description of these observables, a simulation of VBS+j at NLO accuracy, currently unavailable but within the reach of modern automated tools, is certainly desirable.

7 Conclusion

- Sum-up of the study.

[MP: This might deserve a section on its own.]
Recommendations to experimental collaborations:
- Combinations with EW NLO corrections.
- Missing higher EW order: $\pm\delta^2_{\mathrm{NLOEW}}$
- Systematics when using NLO QCD approximation
- Systematics of different parton shower
- Combined measurement including EW, QCD, and interference
- Move to NLO predictions / generators
- Comment on the irreducible QCD background
- Uncertainties related to PDF. Some of us have already presented preliminary results on this subjetc []. A forthcoming article will addresses related questions.

Acknowledgements

The authors would like to acknowledge the contribution of the COST Action CA16108 which initiated this work. Moreover, this work was supported by sveral STSM Grant from the COST Action CA16108.
BB, AD, and MP acknowledge financial support by the German Federal Ministry for Education and Research (BMBF) under contract no. 05H15WWCA1 and the German Science Foundation (DFG) under reference number DE 623/6-1.

Appendix A: Appendix one

References

1. **ATLAS** Collaboration, G. Aad *et al.*, *Evidence for Electroweak Production of $W^{\pm}W^{\pm}jj$ in pp Collisions at $\sqrt{s} = 8$ TeV with the ATLAS Detector*. Phys. Rev. Lett. **113** (2014) no. 14, 141803, arXiv:1405.6241 [hep-ex].
2. **CMS** Collaboration, V. Khachatryan *et al.*, *Study of vector boson scattering and search for new physics in events with two same-sign leptons and two jets*. Phys. Rev. Lett. **114** (2015) no. 5, 051801, arXiv:1410.6315 [hep-ex].
3. **CMS** Collaboration, A. M. Sirunyan *et al.*, *Observation of electroweak production of same-sign W boson pairs in the two jet and two same-sign lepton final state in proton-proton collisions at $\sqrt{s} = 13$ TeV*. arXiv:1709.05822 [hep-ex].
4. **ATLAS** Collaboration, M. Aaboud *et al.*, *Measurement of $W^{\pm}W^{\pm}$ vector-boson scattering and limits on anomalous quartic gauge couplings with the ATLAS detector*. Phys. Rev. **D96** (2017) 012007, arXiv:1611.02428 [hep-ex].
5. B. Jager, C. Oleari, and D. Zeppenfeld, *Next-to-leading order QCD corrections to W+W- production via vector-boson fusion*. JHEP **07** (2006) 015, arXiv:hep-ph/0603177 [hep-ph].
6. B. Jager, C. Oleari, and D. Zeppenfeld, *Next-to-leading order QCD corrections to Z boson pair production via vector-boson fusion*. Phys. Rev. **D73** (2006) 113006, arXiv:hep-ph/0604200 [hep-ph].
7. G. Bozzi, B. Jager, C. Oleari, and D. Zeppenfeld, *Next-to-leading order QCD corrections to W+ Z*

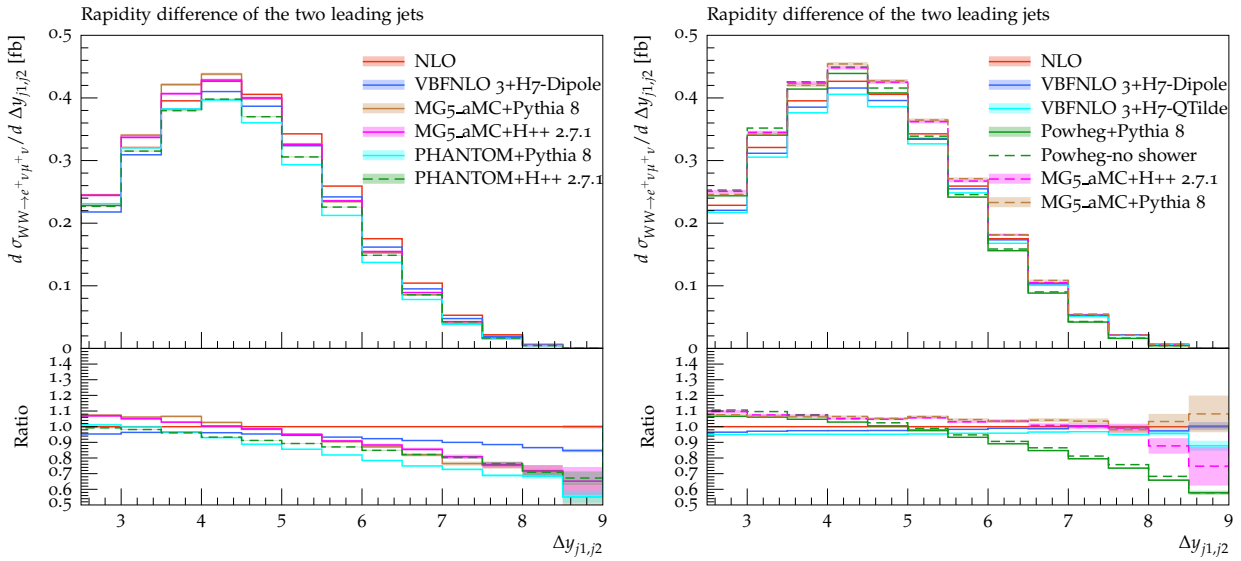

Fig. 16: Same as in Fig. 14, for the rapidity separation of the two tagging jets.

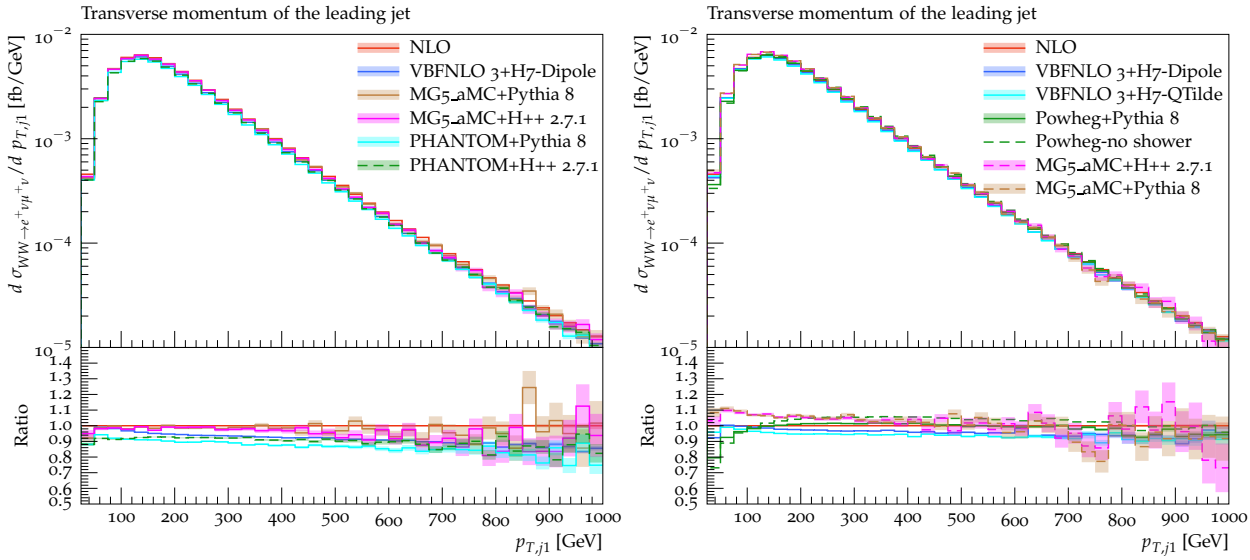

Fig. 17: Same as in Fig. 14, for the transverse momentum of the hardest jet.

and W- Z production via vector-boson fusion. Phys. Rev. **D75** (2007) 073004, arXiv:hep-ph/0701105 [hep-ph].

8. B. Jäger, C. Oleari, and D. Zeppenfeld, *Next-to-leading order QCD corrections to W^+W^+jj and W^-W^-jj production via weak-boson fusion.* Phys. Rev. **D80** (2009) 034022, arXiv:0907.0580 [hep-ph].
9. B. Jäger and G. Zanderighi, *NLO corrections to electroweak and QCD production of W^+W^+ plus two jets in the POWHEGBOX.* JHEP **11** (2011) 055, arXiv:1108.0864 [hep-ph].
10. A. Denner, L. Hošeková, and S. Kallweit, *NLO QCD corrections to W^+W^+jj production in vector-boson fusion at the LHC.* Phys. Rev. **D86** (2012) 114014, arXiv:1209.2389 [hep-ph].
11. M. Rauch, *Vector-Boson Fusion and Vector-Boson Scattering.* arXiv:1610.08420 [hep-ph].
12. T. Melia, K. Melnikov, R. Röntsch, and G. Zanderighi, *Next-to-leading order QCD predictions for W^+W^+jj production at the LHC.* JHEP **12** (2010) 053, arXiv:1007.5313 [hep-ph].
13. T. Melia, P. Nason, R. Röntsch, and G. Zanderighi, *W^+W^+ plus dijet production in*

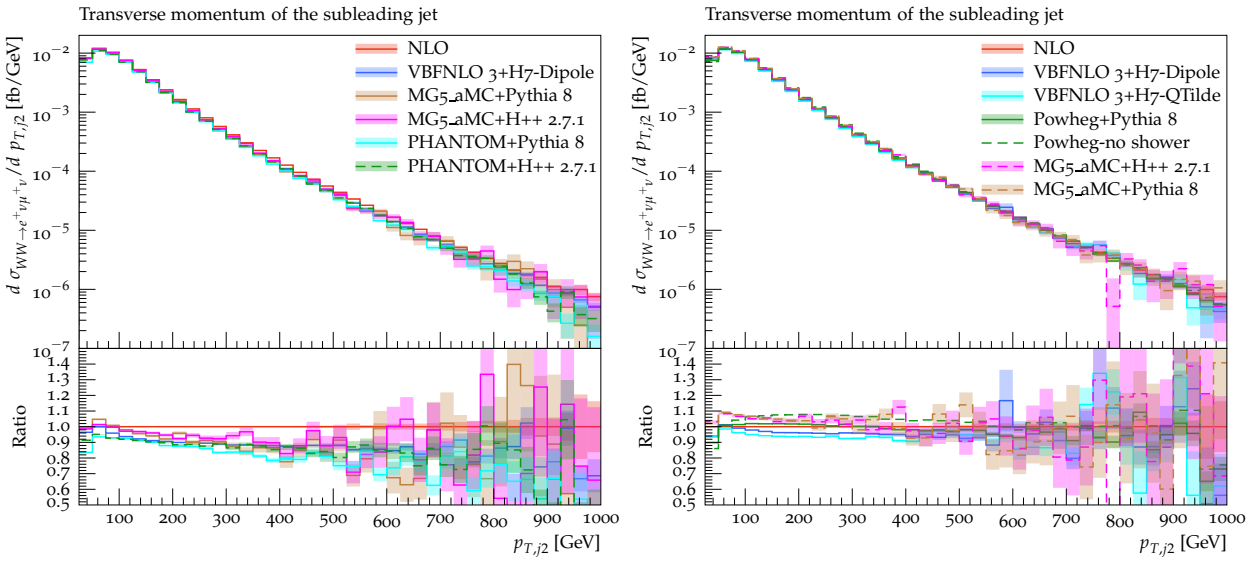

Fig. 18: Same as in Fig. 14, for the transverse momentum of the second-hardest jet.

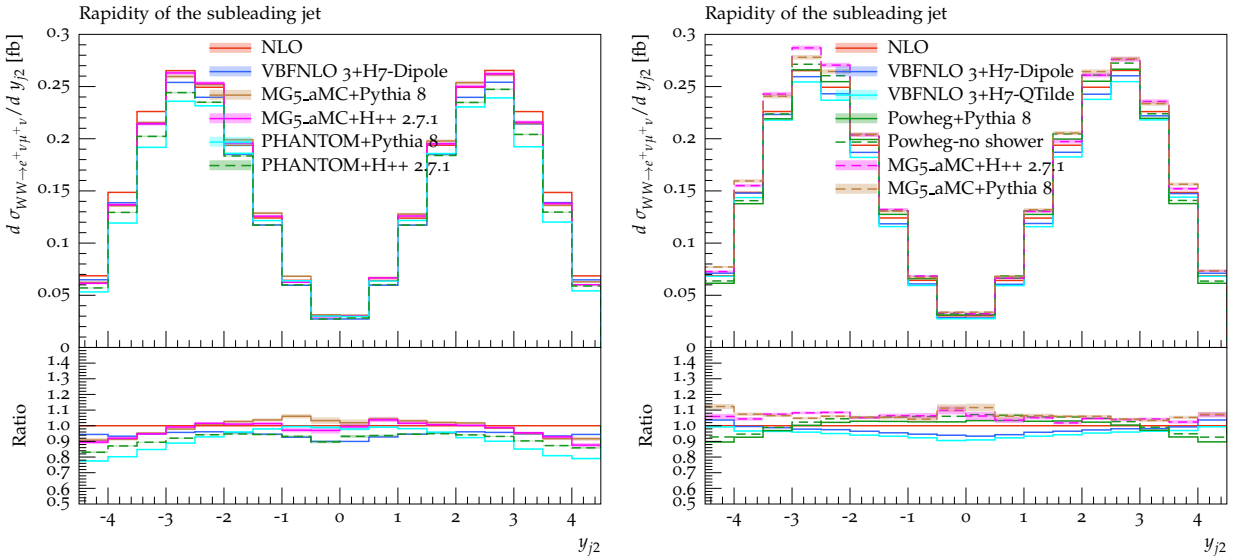

Fig. 19: Same as in Fig. 14, for the rapidity of the second-hardest jet.

the POWHEGBOX. Eur. Phys. J. **C71** (2011) 1670, arXiv:1102.4846 [hep-ph].

14. F. Campanario, M. Kerner, L. D. Ninh, and D. Zeppenfeld, *Next-to-leading order QCD corrections to W^+W^+ and W^-W^- production in association with two jets*. Phys. Rev. **D89** (2014) no. 5, 054009, arXiv:1311.6738 [hep-ph].
15. J. Baglio *et al.*, *Release Note - VBFNLO 2.7.0*. arXiv:1404.3940 [hep-ph].
16. B. Biedermann, A. Denner, and M. Pellen, *Complete NLO corrections to W^+W^+ scattering and its irreducible background at the LHC*. JHEP **10** (2017) 124, arXiv:1708.00268 [hep-ph].
17. C. F. Anders *et al.*, "VBSCan Split 2017 Workshop Summary," 2018. arXiv:1801.04203 [hep-ph].
18. B. Biedermann, A. Denner, and M. Pellen, *Large electroweak corrections to vector-boson scattering at the Large Hadron Collider*. Phys. Rev. Lett. **118** (2017) no. 26, 261801, arXiv:1611.02951 [hep-ph].
19. M. Rauch and S. PlÃďtzer, *Parton Shower Matching Systematics in Vector-Boson-Fusion WW Production*. Eur. Phys. J. **C77** (2017) no. 5, 293, arXiv:1605.07851 [hep-ph].

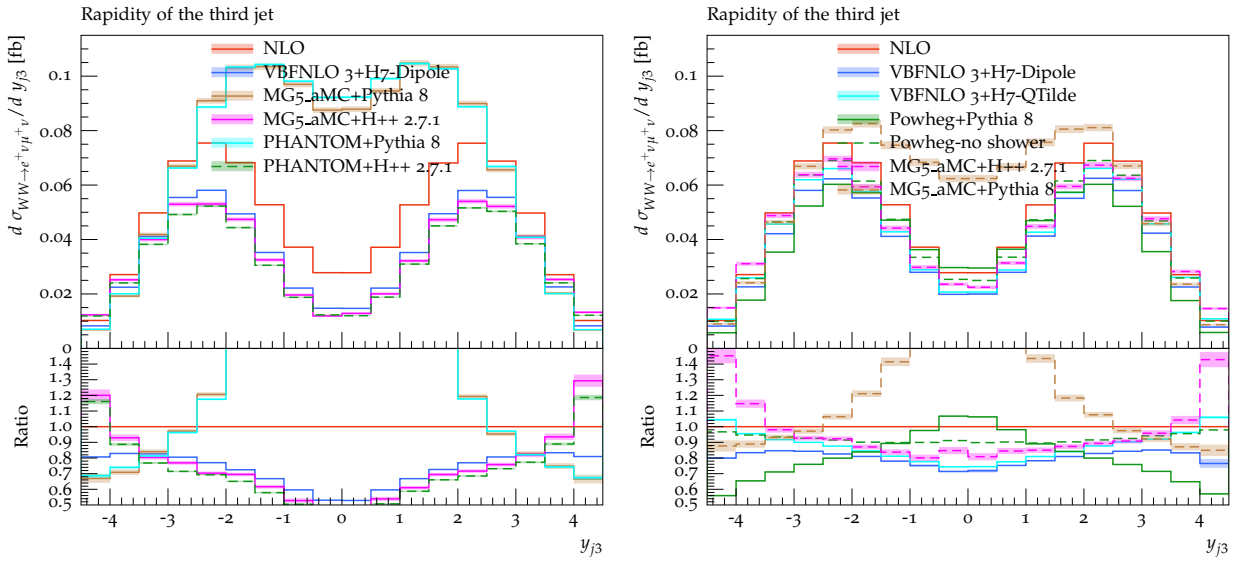

Fig. 20: Same as in Fig. 14, for the rapidity of the third-hardest jet.

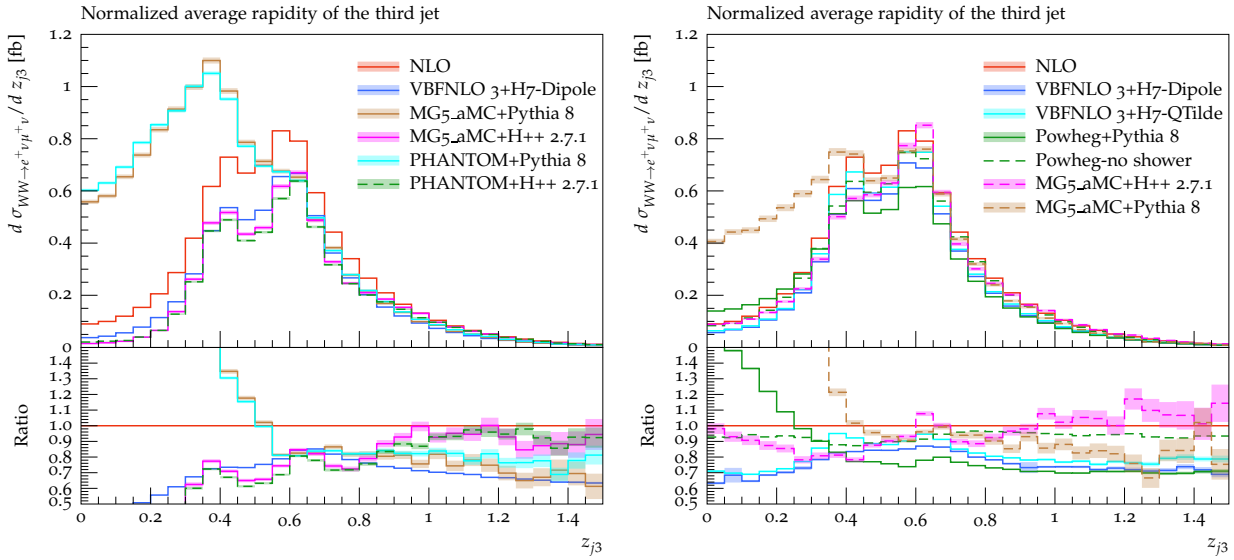

Fig. 21: Same as in Fig. 14, for the z variable of the third-hardest jet.

20. S. Frixione and B. R. Webber, *Matching NLO QCD computations and parton shower simulations*. JHEP **06** (2002) 029, arXiv:hep-ph/0204244 [hep-ph].
21. P. Nason, *A New method for combining NLO QCD with shower Monte Carlo algorithms*. JHEP **11** (2004) 040, arXiv:hep-ph/0409146 [hep-ph].
22. S. Frixione, P. Nason, and C. Oleari, *Matching NLO QCD computations with Parton Shower simulations: the POWHEG method*. JHEP **11** (2007) 070, arXiv:0709.2092 [hep-ph].
23. J. Bellm *et al.*, *Herwig 7.0/Herwig++ 3.0 release note*. Eur. Phys. J. **C76** (2016) no. 4, 196, arXiv:1512.01178 [hep-ph].
24. I. Kuss and H. Spiesberger, *Luminosities for vector boson - vector boson scattering at high-energy colliders*. Phys. Rev. **D53** (1996) 6078–6093, arXiv:hep-ph/9507204 [hep-ph].
25. E. Accomando, A. Denner, and S. Pozzorini, *Logarithmic electroweak corrections to $e^+e^- \to \nu_e\bar{\nu}_e W^+W^-$*. JHEP **03** (2007) 078, arXiv:hep-ph/0611289 [hep-ph].
26. S. Dawson, *The Effective W Approximation*. Nucl. Phys. **B249** (1985) 42–60.
27. M. J. Duncan, G. L. Kane, and W. W. Repko, *W W Physics at Future Colliders*. Nucl. Phys. **B272**

(1986) 517–559.
28. R. N. Cahn and S. Dawson, *Production of Very Massive Higgs Bosons*. Phys. Lett. **136B** (1984) 196. [Erratum: Phys. Lett.138B,464(1984)].
29. S. Dittmaier and C. Schwan, *Non-factorizable photonic corrections to resonant production and decay of many unstable particles*. Eur. Phys. J. **C76** (2016) no. 3, 144, arXiv:1511.01698 [hep-ph].
30. S. Dittmaier and M. Roth, *LUSIFER: A LUcid approach to six FERmion production*. Nucl. Phys. **B642** (2002) 307–343, arXiv:hep-ph/0206070 [hep-ph].
31. A. Denner, S. Dittmaier, and L. Hofer, *COLLIER - A fortran-library for one-loop integrals*. PoS **LL2014** (2014) 071, arXiv:1407.0087 [hep-ph].
32. A. Denner, S. Dittmaier, and L. Hofer, COLLIER*: a fortran-based Complex One-Loop LIbrary in Extended Regularizations*. Comput. Phys. Commun. **212** (2017) 220–238, arXiv:1604.06792 [hep-ph].
33. J. Alwall *et al.*, *The automated computation of tree-level and next-to-leading order differential cross sections, and their matching to parton shower simulations*. JHEP **07** (2014) 079, arXiv:1405.0301 [hep-ph].
34. S. Frixione, Z. Kunszt, and A. Signer, *Three jet cross-sections to next-to-leading order*. Nucl. Phys. **B467** (1996) 399–442, arXiv:hep-ph/9512328 [hep-ph].
35. S. Frixione, *A General approach to jet cross-sections in QCD*. Nucl. Phys. **B507** (1997) 295–314, arXiv:hep-ph/9706545 [hep-ph].
36. R. Frederix, S. Frixione, F. Maltoni, and T. Stelzer, *Automation of next-to-leading order computations in QCD: The FKS subtraction*. JHEP **10** (2009) 003, arXiv:0908.4272 [hep-ph].
37. R. Frederix, S. Frixione, A. S. Papanastasiou, S. Prestel, and P. Torrielli, *Off-shell single-top production at NLO matched to parton showers*. JHEP **06** (2016) 027, arXiv:1603.01178 [hep-ph].
38. G. Ossola, C. G. Papadopoulos, and R. Pittau, *Reducing full one-loop amplitudes to scalar integrals at the integrand level*. Nucl. Phys. **B763** (2007) 147–169, arXiv:hep-ph/0609007 [hep-ph].
39. P. Mastrolia, E. Mirabella, and T. Peraro, *Integrand reduction of one-loop scattering amplitudes through Laurent series expansion*. JHEP **06** (2012) 095, arXiv:1203.0291 [hep-ph]. [Erratum: JHEP11,128(2012)].
40. G. Passarino and M. J. G. Veltman, *One-loop corrections for e^+e^- annihilation into $\mu^+\mu^-$ in the Weinberg model*. Nucl. Phys. **B160** (1979) 151–207.
41. A. I. Davydychev, *A Simple formula for reducing Feynman diagrams to scalar integrals*. Phys. Lett. **B263** (1991) 107–111.
42. A. Denner and S. Dittmaier, *Reduction schemes for one-loop tensor integrals*. Nucl. Phys. **B734** (2006) 62–115, hep-ph/0509141.
43. V. Hirschi, R. Frederix, S. Frixione, M. V. Garzelli, F. Maltoni, and R. Pittau, *Automation of one-loop QCD corrections*. JHEP **05** (2011) 044, arXiv:1103.0621 [hep-ph].
44. G. Ossola, C. G. Papadopoulos, and R. Pittau, *CutTools: A Program implementing the OPP reduction method to compute one-loop amplitudes*. JHEP **03** (2008) 042, arXiv:0711.3596 [hep-ph].
45. T. Peraro, *Ninja: Automated Integrand Reduction via Laurent Expansion for One-Loop Amplitudes*. Comput. Phys. Commun. **185** (2014) 2771–2797, arXiv:1403.1229 [hep-ph].
46. V. Hirschi and T. Peraro, *Tensor integrand reduction via Laurent expansion*. JHEP **06** (2016) 060, arXiv:1604.01363 [hep-ph].
47. H.-S. Shao, *Iregi user manual, unpublished*.
48. F. Cascioli, P. Maierhöfer, and S. Pozzorini, *Scattering Amplitudes with Open Loops*. Phys. Rev. Lett. **108** (2012) 111601, arXiv:1111.5206 [hep-ph].
49. A. Ballestrero, A. Belhouari, G. Bevilacqua, V. Kashkan, and E. Maina, *PHANTOM: A Monte Carlo event generator for six parton final states at high energy colliders*. Comput. Phys. Commun. **180** (2009) 401–417, arXiv:0801.3359 [hep-ph].
50. A. Denner and S. Dittmaier, *The Complex-mass scheme for perturbative calculations with unstable particles*. Nucl. Phys. Proc. Suppl. **160** (2006) 22–26, arXiv:hep-ph/0605312 [hep-ph]. [,22(2006)].
51. A. Ballestrero, "PHACT: Helicity amplitudes for present and future colliders," in *High energy physics and quantum field theory. Proceedings, 14th International Workshop, QFTHEP'99, Moscow, Russia, May 27-June 2, 1999*, pp. 303–309. 1999. arXiv:hep-ph/9911318 [hep-ph].
52. A. Ballestrero and E. Maina, *A New method for helicity calculations*. Phys. Lett. **B350** (1995) 225–233, arXiv:hep-ph/9403244 [hep-ph].
53. F. A. Berends, P. H. Daverveldt, and R. Kleiss, *Complete Lowest Order Calculations for Four*

Lepton Final States in electron-Positron Collisions. Nucl. Phys. **B253** (1985) 441–463.
54. G. P. Lepage, *A New Algorithm for Adaptive Multidimensional Integration*. J. Comput. Phys. **27** (1978) 192.
55. S. Alioli, P. Nason, C. Oleari, and E. Re, *A general framework for implementing NLO calculations in shower Monte Carlo programs: the POWHEG BOX*. JHEP **06** (2010) 043, arXiv:1002.2581 [hep-ph].
56. K. Arnold *et al.*, *VBFNLO: A Parton level Monte Carlo for processes with electroweak bosons*. Comput. Phys. Commun. **180** (2009) 1661–1670, arXiv:0811.4559 [hep-ph].
57. K. Arnold *et al.*, *VBFNLO: A Parton Level Monte Carlo for Processes with Electroweak Bosons – Manual for Version 2.5.0*. arXiv:1107.4038 [hep-ph].
58. S. Actis *et al.*, *Recursive generation of one-loop amplitudes in the Standard Model*. JHEP **04** (2013) 037, arXiv:1211.6316 [hep-ph].
59. S. Actis *et al.*, *RECOLA: REcursive Computation of One-Loop Amplitudes*. Comput. Phys. Commun. **214** (2017) 140–173, arXiv:1605.01090 [hep-ph].
60. S. Catani and M. H. Seymour, *A general algorithm for calculating jet cross-sections in NLO QCD*. Nucl. Phys. **B485** (1997) 291–419, arXiv:hep-ph/9605323 [hep-ph]. [Erratum: Nucl. Phys. **B510** (1998) 503].
61. S. Dittmaier, *A general approach to photon radiation off fermions*. Nucl. Phys. **B565** (2000) 69–122, arXiv:hep-ph/9904440.
62. A. Denner and R. Feger, *NLO QCD corrections to off-shell top-antitop production with leptonic decays in association with a Higgs boson at the LHC*. JHEP **11** (2015) 209, arXiv:1506.07448 [hep-ph].
63. A. Denner, J.-N. Lang, M. Pellen, and S. Uccirati, *Higgs production in association with off-shell top-antitop pairs at NLO EW and QCD at the LHC*. JHEP **02** (2017) 053, arXiv:1612.07138 [hep-ph].
64. F. A. Berends, R. Pittau, and R. Kleiss, *All electroweak four fermion processes in electron - positron collisions*. Nucl. Phys. **B424** (1994) 308–342, arXiv:hep-ph/9404313 [hep-ph].
65. A. Denner *et al.*, *Predictions for all processes $e^+e^- \to 4\,fermions + \gamma$*. Nucl. Phys. **B560** (1999) 33–65, arXiv:hep-ph/9904472.
66. M. Moretti, T. Ohl, and J. Reuter, *O'Mega: An Optimizing matrix element generator*. arXiv:hep-ph/0102195 [hep-ph].
67. W. Kilian, T. Ohl, and J. Reuter, *WHIZARD: Simulating Multi-Particle Processes at LHC and ILC*. Eur. Phys. J. **C71** (2011) 1742, arXiv:0708.4233 [hep-ph].
68. **NNPDF** Collaboration, R. D. Ball *et al.*, *Parton distributions for the LHC Run II*. JHEP **04** (2015) 040, arXiv:1410.8849 [hep-ph].
69. A. Buckley, J. Ferrando, S. Lloyd, K. Nordström, B. Page, M. Rüfenacht, M. Schönherr, and G. Watt, *LHAPDF6: parton density access in the LHC precision era*. Eur. Phys. J. **C75** (2015) 132, arXiv:1412.7420 [hep-ph].
70. D. Yu. Bardin, A. Leike, T. Riemann, and M. Sachwitz, *Energy-dependent width effects in e^+e^--annihilation near the Z-boson pole*. Phys. Lett. **B206** (1988) 539–542.
71. A. Denner, S. Dittmaier, M. Roth, and D. Wackeroth, *Electroweak radiative corrections to $e^+e^- \to WW \to 4$ fermions in double-pole approximation: The RACOONWW approach*. Nucl. Phys. **B587** (2000) 67–117, arXiv:hep-ph/0006307 [hep-ph].
72. A. Denner *et al.*, *Electroweak corrections to charged-current $e^+e^- \to 4$ fermion processes: Technical details and further results*. Nucl. Phys. **B724** (2005) 247–294, arXiv:hep-ph/0505042.
73. **CMS** Collaboration, *Observation of electroweak production of same-sign W boson pairs in the two jet and two same-sign lepton final state in proton-proton collisions at 13 TeV*. CMS-PAS-SMP-17-004.
74. M. Cacciari, G. P. Salam, and G. Soyez, *The anti-k_t jet clustering algorithm*. JHEP **04** (2008) 063, arXiv:0802.1189 [hep-ph].
75. T. Sjöstrand, S. Ask, J. R. Christiansen, R. Corke, N. Desai, P. Ilten, S. Mrenna, S. Prestel, C. O. Rasmussen, and P. Z. Skands, *An Introduction to PYTHIA 8.2*. Comput. Phys. Commun. **191** (2015) 159–177, arXiv:1410.3012 [hep-ph].
76. M. Bahr *et al.*, *Herwig++ Physics and Manual*. Eur. Phys. J. **C58** (2008) 639–707, arXiv:0803.0883 [hep-ph].
77. J. Bellm *et al.*, *Herwig++ 2.7 Release Note*. arXiv:1310.6877 [hep-ph].
78. S. Platzer and S. Gieseke, *Dipole Showers and Automated NLO Matching in Herwig++*. Eur. Phys. J. **C72** (2012) 2187, arXiv:1109.6256 [hep-ph].
79. J. Bellm *et al.*, *Herwig 7.1 Release Note*. arXiv:1705.06919 [hep-ph].
80. T. Binoth *et al.*, *A Proposal for a standard interface between Monte Carlo tools and one-loop programs*. Comput. Phys. Commun. **181** (2010)

1612–1622, arXiv:1001.1307 [hep-ph]. [,1(2010)].

81. S. Alioli *et al.*, *Update of the Binoth Les Houches Accord for a standard interface between Monte Carlo tools and one-loop programs*. Comput. Phys. Commun. **185** (2014) 560–571, arXiv:1308.3462 [hep-ph].
82. J. R. Andersen *et al.*, *Les Houches 2013: Physics at TeV Colliders: Standard Model Working Group Report*. arXiv:1405.1067 [hep-ph].
83. P. Skands, S. Carrazza, and J. Rojo, *Tuning PYTHIA 8.1: the Monash 2013 Tune*. Eur. Phys. J. **C74** (2014) no. 8, 3024, arXiv:1404.5630 [hep-ph].
84. P. Artoisenet, R. Frederix, O. Mattelaer, and R. Rietkerk, *Automatic spin-entangled decays of heavy resonances in Monte Carlo simulations*. JHEP **03** (2013) 015, arXiv:1212.3460 [hep-ph].

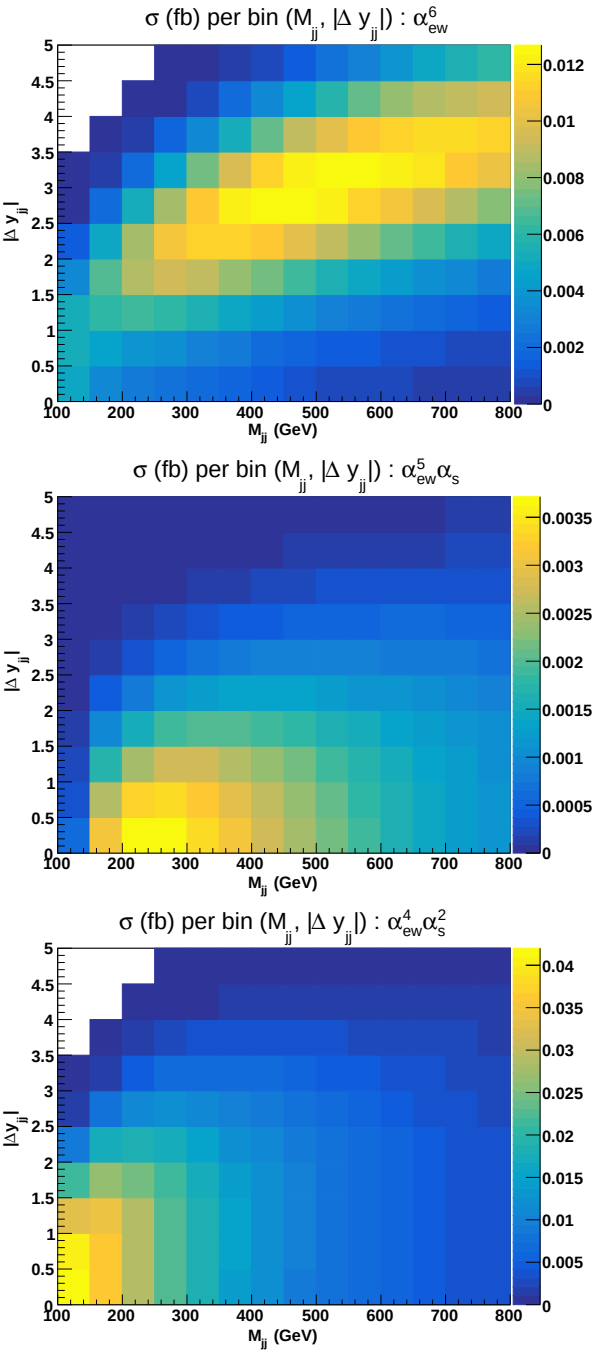

Fig. 3: Cross sections (fb) per bin in the plan $(m_{\rm jj}, \Delta y_{\rm jj})$ for the three LO contributions of orders $\mathcal{O}(\alpha^6)$ (top), $\mathcal{O}(\alpha_{\rm s}\alpha^5)$ (middle), and $\mathcal{O}(\alpha_{\rm s}^2\alpha^4)$ (bottom). [MP: On the plots: it should be α and not α_{em} and $m_{\rm jj}$ instead of M_{jj}. And we have the convention to put $\alpha_{\rm s}$ before α.]

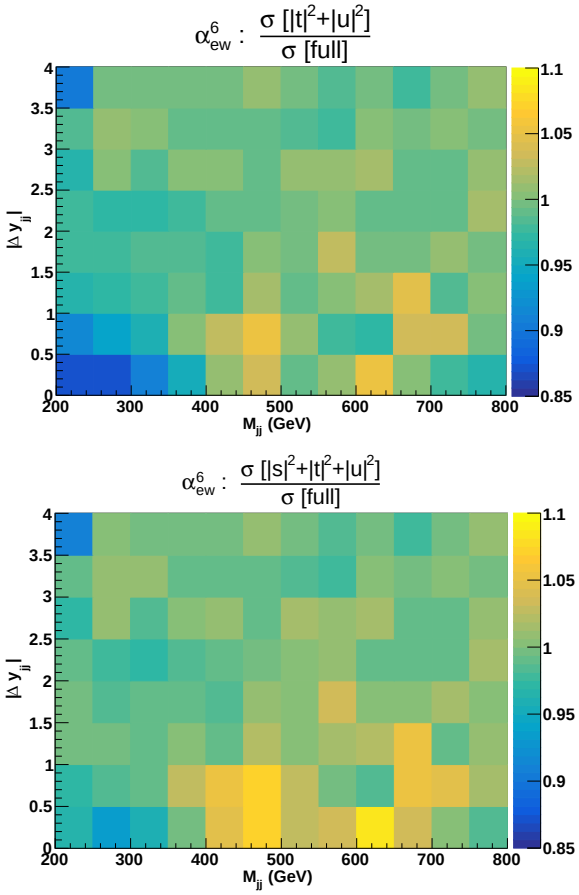

Fig. 4: Cross sections (fb) per bin in the plan $(m_{jj}, |\Delta y_{jj}|)$ at order $\mathcal{O}(\alpha^6)$. Ratio of approximated squared amplitudes over the full matrix element. The approximated squared amplitudes are computed as $|\mathcal{A}|^2 \sim |t|^2 + |u|^2$ (top) and $|\mathcal{A}|^2 \sim |s|^2 + |t|^2 + |u|^2$ (bottom).

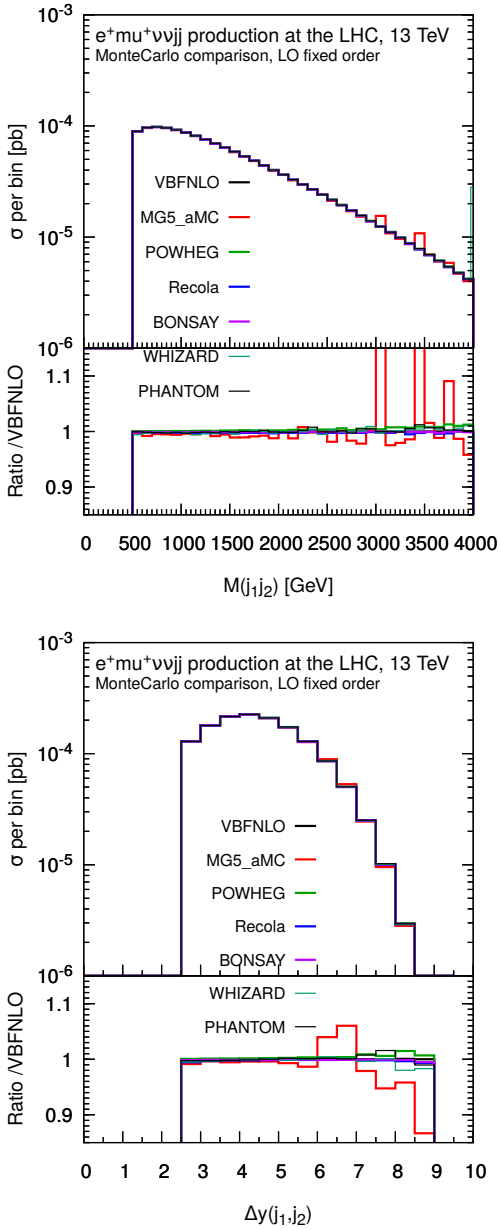

Fig. 5: Differential distributions in the invariant mass (top) and rapidity difference of the two tagging jets (bottom). The LHC process considered is pp $\to \mu^+\nu_\mu e^+\nu_e jj$ at LO accuracy and order $\mathcal{O}(\alpha^6)$. The description of the different programs used can be found in Sec. 3.2. The upper plots provides the absolute value for each prediction while the lower plots presents all predictions normalised to MoCaNLO+Recola which is one of the full predictions. The predictions are obtained in the fiducial region described in Sec. 3.3. [MP: MG statistics should be improved and the baseline changed to Recola.]

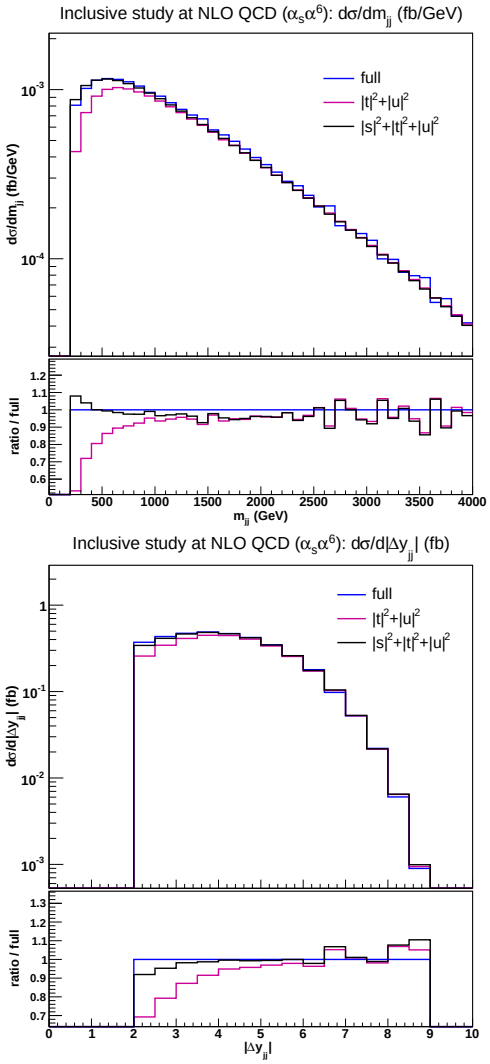

Fig. 6: Differential distributions in $m_{\rm jj}$ (left) and $|\Delta y_{\rm jj}|$ (right) at NLO QCD *i.e.* at order $\mathcal{O}(\alpha_{\rm s}\alpha^6)$ for the full computation and two approximations. In addition to the cuts of Sec. 3.3, the VBS cuts take the values: $m_{\rm jj} > 200\,\text{GeV}$ and $|\Delta y_{\rm jj}| > 2$.

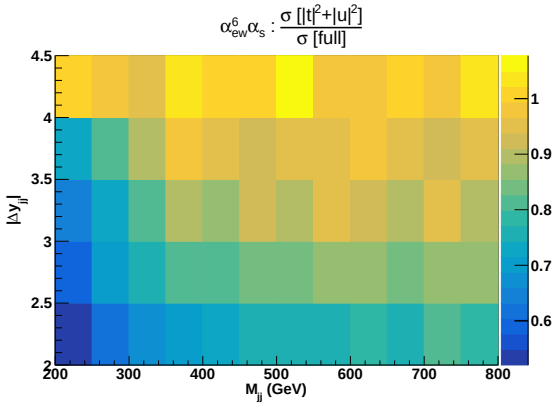

Fig. 7: Ratio of cross sections (fb) per bin of $(m_{\rm jj}, |\Delta y_{\rm jj}|)$ at NLO QCD *i.e.* at order $\mathcal{O}(\alpha_{\rm s}\alpha^6)$ for the VBS approximation over the full computation. In addition to the cuts of Sec. 3.3, the VBS cuts take the values: $m_{\rm jj} > 200\,\text{GeV}$ and $|\Delta y_{\rm jj}| > 2$. **GP: notation to be changed, Mjj -> mjj, alphas alpha**

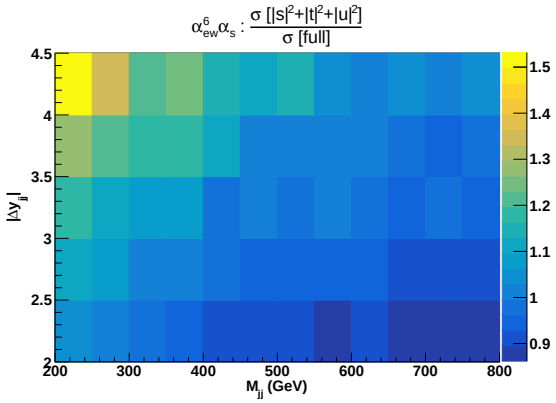

Fig. 8: Ratio of cross sections (fb) per bin of $(m_{\rm jj}, |\Delta y_{\rm jj}|)$ at NLO QCD *i.e.* at order $\mathcal{O}(\alpha_{\rm s}\alpha^6)$ for the VBS approximation with s-channel contributions over the full computation. In addition to the cuts of Sec. 3.3, the VBS cuts take the values: $m_{\rm jj} > 200\,\text{GeV}$ and $|\Delta y_{\rm jj}| > 2$. **GP: notation to be changed, Mjj -> mjj, alphas alpha**

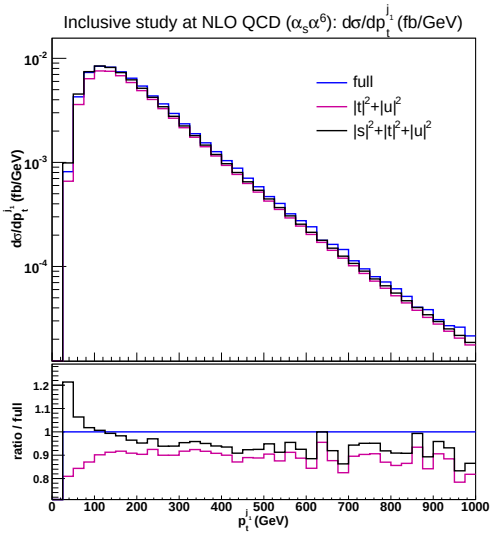

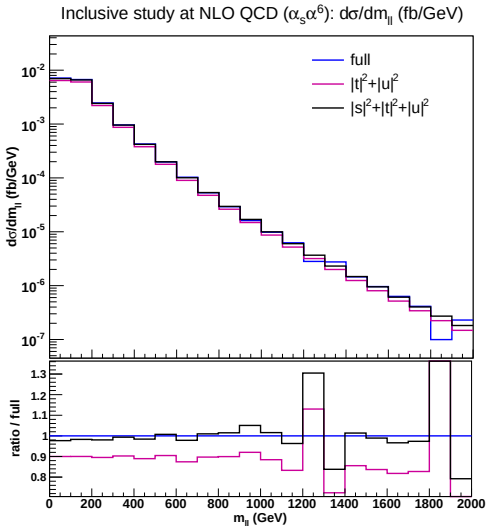

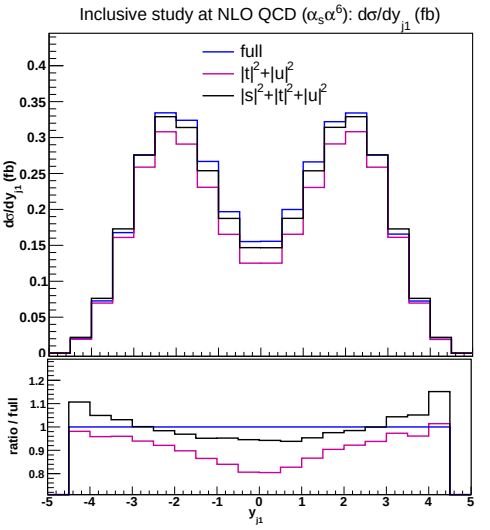

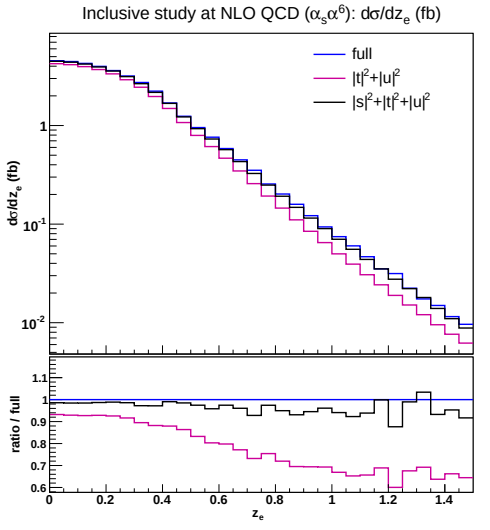

Fig. 9: Differential distributions in the transverse momentum and rapidity of the hardest tagging jet at NLO QCD *i.e.* at order $\mathcal{O}(\alpha_s\alpha^6)$ for the full computation and two approximations. In addition to the cuts of Sec. 3.3, the VBS cuts take the values: $m_{jj} > 200\,\text{GeV}$ and $|\Delta y_{jj}| > 2$.

Fig. 10: Differential distributions in the lepton-lepton invariant mass and the electron Zeppenfeld variable at NLO QCD *i.e.* at order $\mathcal{O}(\alpha_s\alpha^6)$ for the full computation and two approximations. In addition to the cuts of Sec. 3.3, the VBS cuts take the values: $m_{jj} > 200\,\text{GeV}$ and $|\Delta y_{jj}| > 2$.

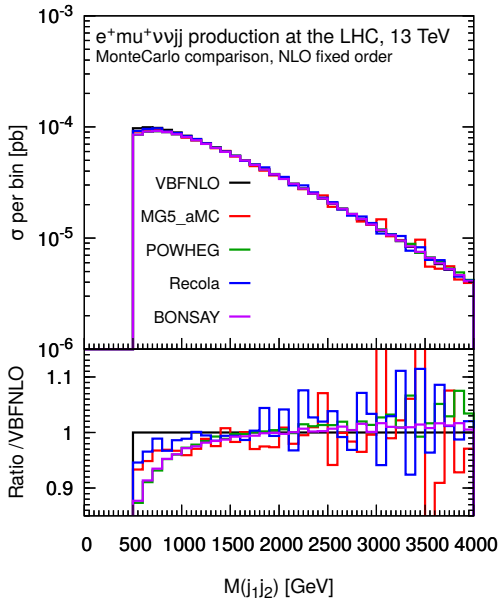

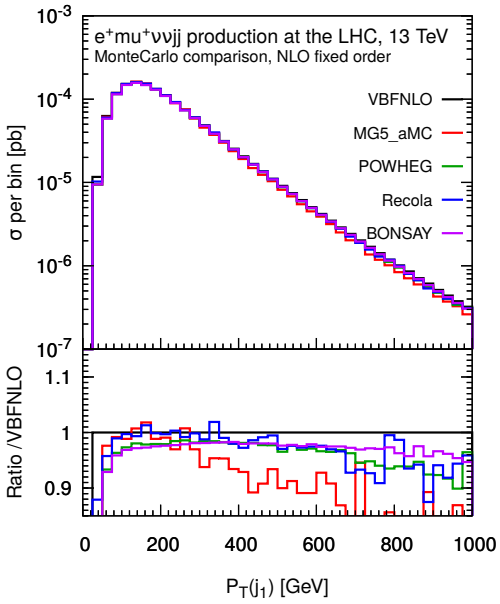

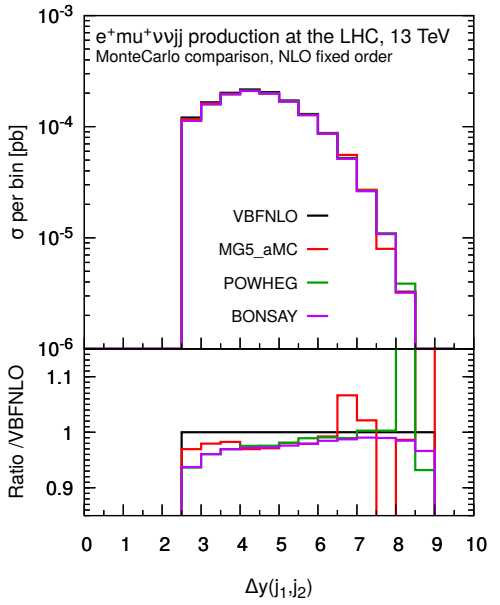

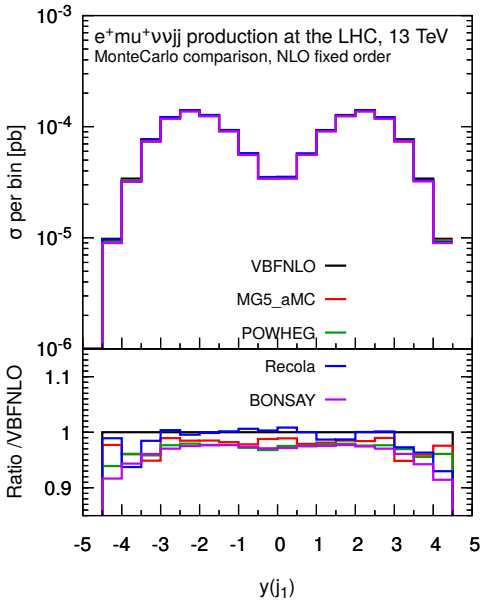

Fig. 11: Differential distributions in the invariant mass (top) and rapidity difference of the two tagging jets (bottom). The LHC process considered is pp $\to \mu^+\nu_\mu e^+\nu_e jj$ at NLO accuracy and order $\mathcal{O}(\alpha_s\alpha^6)$. The description of the different programs used can be found in Sec. 3.2. The upper plots provides the absolute value for each prediction while the lower plots presents all predictions normalised to MoCaNLO+Recola which is one of the full predictions. The predictions are obtained in the fiducial region described in Sec. 3.3. [MP: MG statistics should be improved and the baseline changed to Recola.]

Fig. 12: Differential distributions in the transverse momentum (top) and rapidity of the hardest jet (bottom). The LHC process considered is pp $\to \mu^+\nu_\mu e^+\nu_e jj$ at NLO accuracy and order $\mathcal{O}(\alpha_s\alpha^6)$. The description of the different programs used can be found in Sec. 3.2. The upper plots provides the absolute value for each prediction while the lower plots presents all predictions normalised to MoCaNLO+Recola which is one of the full predictions. The predictions are obtained in the fiducial region described in Sec. 3.3. [MP: MG statistics should be improved and the baseline changed to Recola.]

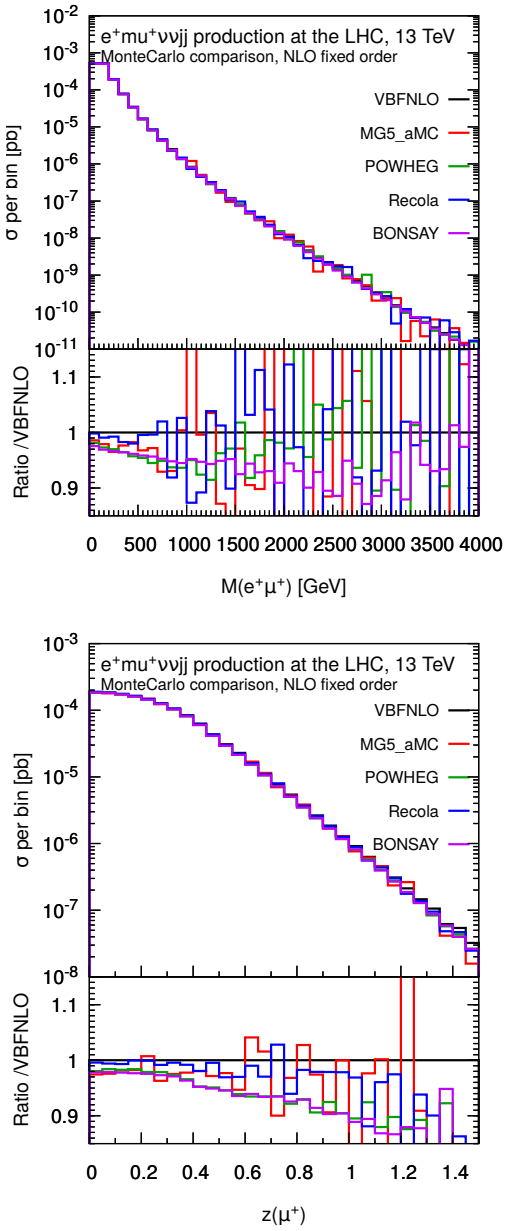

Fig. 13: Differential distributions in the invariant mass of the two charged leptons (top) and Zeppenfeld variable for the muon (bottom). The LHC process considered is pp $\to \mu^+\nu_\mu e^+\nu_e jj$ at NLO accuracy and order $\mathcal{O}(\alpha_s\alpha^6)$. The description of the different programs used can be found in Sec. 3.2. The upper plots provides the absolute value for each prediction while the lower plots presents all predictions normalised to MoCaNLO+Recola which is one of the full predictions. The predictions are obtained in the fiducial region described in Sec. 3.3. [MP: MG statistics should be improved and the baseline changed to Recola.]